İzzet Güzelkara

M.Sc. Thesis

AGU 2024

DESIGN AND PERFORMANCE ENHANCEMENT OF AN ULTRA WIDEBAND VIVALDI ANTENNA

M.Sc. THESIS
SUBMITTED TO THE DEPARTMENT OF ELECTRICAL AND COMPUTER ENGINEERING
AND THE GRADUATE SCHOOL OF ENGINEERING AND SCIENCE
OF ABDULLAH GUL UNIVERSITY
IN PARTIAL FULFILLMENT OF THE REQUIREMENTS
FOR THE DEGREE OF
MASTER OF SCIENCE

By
İzzet Güzelkara
September 2024

DESIGN AND PERFORMANCE ENHANCEMENT OF AN ULTRA WIDEBAND VIVALDI ANTENNA

A THESIS
SUBMITTED TO THE DEPARTMENT OF ELECTRICAL AND COMPUTER ENGINEERING
AND THE GRADUATE SCHOOL OF ENGINEERING AND SCIENCE OF ABDULLAH GUL UNIVERSITY
IN PARTIAL FULFILLMENT OF THE REQUIREMENTS
FOR THE DEGREE OF
MASTER OF SCIENCE

By
İzzet Güzelkara
September 2024

SCIENTIFIC ETHICS COMPLIANCE

I hereby declare that all information in this document has been obtained in accordance with academic rules and ethical conduct. I also declare that, as required by these rules and conduct, I have fully cited and referenced all materials and results that are not original to this work.

Name-Surname: İzzet Güzelkara
Signature :

REGULATORY COMPLIANCE

M.Sc. thesis titled Design and Performance Enhancement of an Ultra Wideband Vivaldi Antenna has been prepared in accordance with the Thesis Writing Guidelines of the Abdullah Gül University, Graduate School of Engineering & Science.

Prepared By	Advisor
İzzet Güzelkara	Asst. Prof. Veli Tayfun Kılıç

Head of the Electrical and Computer Engineering Program

Assoc. Prof. Samet Güler

Signature

ACCEPTANCE AND APPROVAL

M.Sc. thesis titled Design and Performance Enhancement of an Ultra Wideband Vivaldi Antenna and prepared by İzzet Güzelkara has been accepted by the jury in the Electrical and Computer Engineering Graduate Program at Abdullah Gül University, Graduate School of Engineering & Science.

20 / 09 / 2024

(Thesis Defense Exam Date)

JURY:

Advisor : Asst. Prof. Veli Tayfun Kılıç

Member : Prof. Evren Mutlugün

Member : Assoc. Prof. İbrahim Tuna Özdur

APPROVAL:

The acceptance of this M.Sc. thesis has been approved by the decision of the Abdullah Gül University, Graduate School of Engineering & Science, Executive Board dated ….. /….. / …….. and numbered ……..……. .

…….. /…….. / ……..

(Date)

Graduate School Dean
Prof. İrfan ALAN

ABSTRACT

DESIGN AND PERFORMANCE ENHANCEMENT OF AN ULTRA WIDEBAND VIVALDI ANTENNA

İzzet Güzelkara
MSc. in Electrical and Computer Engineering
Advisor: Asst. Prof. Veli Tayfun Kılıç
September 2024

Ultra-wideband technology has become a trending topic in the academic community since 2002 due to the release of the spectral mask by Federal Communications Commission, allowing the use of 3.6-10.1 GHz band for commercial and industrial applications. Being one of the fundamental components of ultra-wideband systems, ultra-wideband antennas are an important research area. In this research, Vivaldi antennas for ultra-wideband communications and several performance enhancement techniques for the antennas were studied. Antennas were designed and simulated using a commercially available three-dimensional electromagnetic simulation tool. First, a simple design of a Vivaldi antenna with a rectangular microstrip feed was obtained. The initial design has a -10 dB impedance bandwidth between 3.1 and 13.6 GHz and an average realized gain of 2.75 dBi. A method based on the alignment of the microstrip feed was described for adjusting the bandwidth of the initial design. Then, using several performance enhancement techniques such as implementation of corrugations and a parasitic patch, the antenna design was improved. Thanks to the applied methods, an antenna design with -10 dB impedance bandwidth extending from 1.33 to 10.1 GHz and an average realized gain of 6 dBi was achieved. Findings of this thesis study show that Vivaldi antennas having specific structures designed with the applied techniques are a promising solution for ultra-wideband communication systems, especially where antennas with directive radiation patterns are desired.

Keywords: Ultra-wideband antenna, Vivaldi, microstrip feed, corrugation, parasitic patch

ÖZET

ULTRA GENİŞ BANTLI VİVALDİ ANTENLERİN TASARIMI VE PERFORMANS İYİLEŞTİRMESİ

İzzet Güzelkara
Elektrik ve Bilgisayar Mühendisliği Anabilim Dalı Yüksek Lisans
Tez Danışmanı: Dr. Öğr. Üyesi Veli Tayfun Kılıç
Eylül 2024

Ultra geniş bant teknolojisi 2002 yılından bu yana akademik camiada popüler bir araştırma konusu haline geldi. Bunun en önemli nedeni, Federal İletişim Komisyonu'nun 2002 yılında yayınladığı ve ultra geniş bant sistemlerinin 3.6-10.1 GHz bandında endüstriyel ve ticari uygulamar için kullanımına izin veren spektral maskedir. Ultra geniş bant sistemlerinin en önemli parçalarından olan antenler de bu nedenle önemli bir araştırma konusu haline gelmiştir. Bu araştırmada, Vivaldi antenlerin ultra geniş bant sistemleri için kullanımı ve antenler üzerinde uygulanan çeşitli performans iyileştirme teknikleri ele alınmıştır. Çalışmada sunulan antenler, ticari erişime açık üç boyutlu bir elektromanyetik simülasyon aracı kullanılarak tasarlanmış ve simüle edilmiştir. İlk olarak, 3.1-13.6 GHz frekansları arasında çalışabilen, bu bantta ortalama 2.75 dBi kazanca sahip ve dikdörtgen şekilli mikroşerit besleme sistemi ile basit bir tasarıma sahip bir Vivaldi anten tasarlanmış, ve mikroşerit beslemenin hizalamasına bağlı olarak bant genişliğinin optimize edildiği bir metod sunulmuştur. Sonrasında, oluklu yüzey ve parazitik yama kullanımı gibi çeşitli performans iyileştirme teknikleri uygulanmış ve antenin tasarımı 1.33 ve 10.1 GHz frekansları arasında çalışabilecek ve bu bantta 6 dBi ortalama kazanca sahip olacak şekilde iyileştirilmiştir. Çalışmanın bulguları, uygulanan tekniklerle tasarlanmış belirli yapılara sahip Vivaldi antenlerin özellikle yönlü radyasyon örüntülerinin arzulandığı ultra geniş bant sistemler için uygun bir seçim olabileceğini sergilemektedir.

Anahtar kelimeler: Ultra geniş bant anten, Vivaldi, mikroşerit besleme, *oluklu yüzey, parazitik yama*

Acknowledgements

I would like to give my sincerest and deepest thanks to my academic advisor, Assistant Professor Veli Tayfun Kılıç, for his guidance and support throughout my studies at Abdullah Gul University. I was lucky to do my graduation project during my bachelor's degree under his and Professor İbrahim Tuna Özdur's supervision, and it has been an honor and a privilege to continue working under him also during my master's degree. He has always provided me and the other students in our radio frequency research group with constant support and guidance.

My colleagues and fellow students in our small radio frequency community, Burakhan Elden, Şaban Duran Şanlıer and Melih Aslan provided valuable inputs and support throughout my studies, and for that I would like to extend my gratitude to them.

I would also like to thank my manager and supervisor from Infineon Technologies Austria AG, Florin Bulhac and Denis Matveev for giving me a chance to do an internship at Infineon Technologies during my master's degree studies. During this internship, I had the chance to hone my skills as an engineer and work alongside an excellent team of fellow engineers and students, and for this I am eternally grateful.

My parents and brothers have always been there for me during all the ups and downs I had throughout my studies. Whenever I faced a hardship, I knew I could count on them for emotional support and love.

TABLE OF CONTENTS

LIST OF FIGURES

LIST OF TABLES

LIST OF ABBREVIATIONS

ADC	Analog to Digital Converter
AVA	Antipodal Vivaldi Antenna
BAVA	Balanced Antipodal Vivaldi Antenna
DAC	Digital to Analog Converter
DARPA	Defence Advanced Research Projects Agency
EIRP	Equivalent Isotropically Radiated Power
ETSA	Exponentially Tapered Slot Antenna
FCC	Federal Communications Commission
ISM	Industrial, Scientific, Medical
LNA	Low Noise Amplifier
MIMO	Multiple Input Multiple Output
OFDM	Orthogonal Frequency Division Multiplexing
RX	Receiver
TX	Transmitter
UWB	Ultra Wideband

Chapter 1

Introduction

1.1 Ultra-wideband technology

In recent years, ultra-wideband (UWB) communications received immense attention both in the industry and the academic community. The technology behind UWB has been known since 1960s and it has been known by various names such as baseband or carrier free communication, impulse radio and nonsinusoidal communication. The term 'ultra-wideband' was first used by the US Department of Defense around 1989, and before that it did not include the aforementioned terms [1]. The earliest applications of UWB found place in military radars and communication systems in the form of pulse communications in which systems a series of pulses of random occurrences to minimize enemy jamming exists [2]. However, UWB technology did not receive significant attention in industrial and commercial applications, as these early applications operated in the unlicensed frequency bands. In 2002, the Federal Communications Commission (FCC) in the United States released a spectral mask which allowed the operation of UWB transmitters in the frequency band between 3.6 GHz and 10.1 GHz [3]. With the release of this new spectral mask, various industrial and commercial applications based on UWB technology was enabled. These applications include but are not limited to:

- High precision ranging at centimeter accuracy [4]
- Asset tracking [5]
- See-through wall imaging [6]
- High speed broadband internet access
- Newly emerging applications that require extremely low latency and high data rates such as virtual and augmented reality [7]

The applications mentioned above operate at different frequencies within the UWB spectrum. For example, the commercial UWB devices mentioned in [4], which are used for high precision ranging support multiple UWB channels to retrieve phase information

of different signals, so that they can overcome the ambiguity in distance measurements. Some of the common channels used for UWB ranging are UWB channel 5 (6.5 GHz) and channel 9 (8 GHz). It should be noted that the different UWB channels are not active at the same time, but rather the devices ensure agile switching between the UWB channels to retrieve phase information of the signals at different frequencies. On the other hand, for UWB see-through-wall radar applications, Office of Communications in the United Kingdom established a standard that allow two bands, one 600 MHz band centered at 4.5 GHz and one 2.5 GHz band centered at 7.25 GHz [6].

Despite its wide variety of usages mentioned above and having a potential for new applications, there are certain limitations of UWB technology. First and foremost, a UWB transmitter must coexist with various narrow band communication standards such as GSM, UMTS, GPS etc. In order to avoid interferences caused by UWB transmitters, FCC regulated the spectral shape and maximum spectral power density of the UWB radiation [8]. The maximum Equivalent Isotropically Radiated Power (EIRP) allowed for UWB radiation is -41.3 dBm or approximately 0.0001 mW/MHz. This indicates that achieving long range communications with UWB transceivers is not an easy task. Another important limitation of the UWB technology is that the short pulses used in the transmitters make it necessary to have ultra fine time resolution in receivers. This can considerably increase the synchronization acquisition time and the complexity of the receiver.

Nevertheless, because of the advantages of operating in ultra-wide frequency band there are several UWB systems that exist today. For example, Qorvo (formerly known as DecaWave), one of the leading companies in UWB technology, offers real time location systems solutions with their wireless semiconductor product DW1000 [9]. Among these solutions there are keyless access to automobiles using proximity measurements, tracking and location of pallets, packages and items in warehouses using absolute location measurements with fixed infrastructure, and tracking of first responders in emergency situations using relative location among a group of nodes measurements. In the application note, different system architectures and implementation methods such as signal strength or time-based schemes depending on the applications are illustrated in detail. NXP is another leading company in UWB technology, and their UWB fine ranging solutions found applications in Samsung cellphones [10]. These applications show that the UWB technology is a promising solution for a variety of upcoming applications in the future.

1. 2 Ultra-wideband antennas

A UWB transceiver consists of several important components such as low noise power amplifiers (LNA), filters, digital to analog (DAC) and analog to digital (ADC) converters. Each of these components play an important role in the modulation and demodulation of the information carrying signal [11]. However, the component that establishes the wireless link between the UWB transmitter and the receiver units is the UWB antenna, which makes it one of the most important parts of a UWB system. A wireless communication between transmitter (TX) and receiver (RX) units together with their parts are illustrated in Figure 1.1. As seen in the figure, electrical signals are converted to electromagnetic waves by the TX antenna. These waves are radiated into space by the TX antenna and some of them are reached to and captured by the RX antenna. In the RX antenna, electromagnetic power is converted into electrical signals and power. Since antennas transmit and receive signals, and also convert electrical signals into electromagnetic waves and vice versa, to achieve robust wireless connectivity, proper antenna selection is critical.

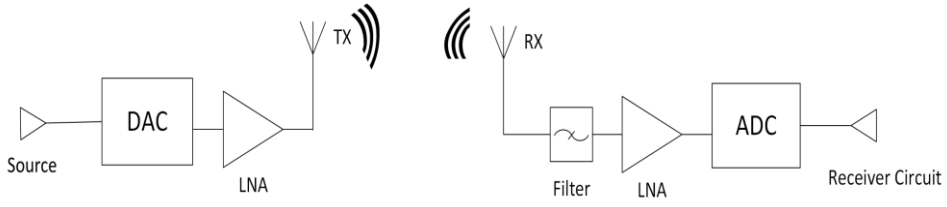

Figure 1.1 A wireless communication between TX and RX units together with their parts

In UWB systems, it is a common practice to employ channel scheduling using Orthogonal Frequency Division Multiplexing (OFDM). OFDM divides the communication into several channels using different time and frequency codes. This method is often used to allocate the available spectrum to a number of users or achieve higher data rates [12]. For applications requiring extremely high data rates more than 1 Gbps, such as high-definition video streaming, Multiple Input Multiple Output (MIMO) technique is also commonly applied with OFDM modulation schemes [13]. In MIMO technique, several antennas that operate at different UWB channels are used. Although

MIMO technique can help achieving great data rates, the drawback of dividing the communication into multiple channels and antennas is that such systems require complex scheduling algorithms. Also, using multiple antennas may come at the expense of larger size, weight and cost. Due to these reasons, MIMO technique with multiple wideband antennas is more common in RF microwave applications, where the antenna sizes are much smaller.

As mentioned above in Section 1.1, the spectrum allocated by FCC for UWB communication is 3.6 GHz to 10.1 GHz. However, before FCC's regulations, the first definition of a UWB signal was brought about by the Defence Advanced Research Projects Agency (DARPA) based on the fractional bandwidth, Bf, of the signal. According to this definition, a signal could be categorized as UWB if the fractional bandwidth is greater than 0.25 which is determined by Equation 1.1

$$B_f = 2\frac{f_h - f_l}{f_h + f_l} \tag{1.1}$$

where f_h and f_l are the highest and lowest cut-off frequencies at which a radiation 3 dB lower than the highest radiated emission is obtained, respectively. Later in 2002, this definition was updated with FCC ruling, such that a signal can be categorized as UWB if it has an instantaneous spectral occupancy of 500 MHz or more, or if the fractional bandwidth is greater than 0.20 determined by Equation 1.1 [14]. For an antenna, this means that the -10 dB impedance bandwidth of the antenna should cover the frequencies between 3.6 GHz and 10.1 GHz. Aside from the bandwidth requirements, another important aspect to consider when choosing an UWB antenna is the transmission and reception characteristics that are imposed by the short pulses used in UWB communications which were discussed above. In order to determine the suitability of an antenna for UWB applications, its transient response can be used to extract useful information such as whether the impulse response of the antenna is short enough or whether the phase center is stable across the UWB frequency range, as described in [15].

There exist several types of antennas, which satisfy the abovementioned requirements, commonly used in UWB systems. Depending on the application, e.g. radar, imaging or communication, each of these antennas has certain advantages and disadvantages. For example, printed monopole patch antennas with a structure shown in Figure 1.2, are designed to have a UWB performance, and they are often suitable for small

handheld devices. Their omnidirectional radiation patterns make printed monopole patch antennas suitable to be used in handheld devices such as mobile phones. This is because of the fact that mobile phone antennas must have 360º angular coverage to receive signals coming from all directions. However, due to their omnidirectional radiation patterns, printed monopole antennas are limited in terms of their gain. Furthermore, design procedures of these antennas to exhibit multiband resonances, which are necessary for an efficient UWB operation may result in complicated structures [16].

On another example, horn antennas are a type of antenna commonly used in UWB systems. Due to their directive radiation patterns and high gain, horn antennas are often preferred for ground penetrating radar and electromagnetic sensing applications [17]. However, these antennas are waveguide-based antennas, such that they are not planar antennas, but rather they have three dimensional (3D) structures. There are horn antennas with various shapes designed to have different properties including polarization type, gain, frequency band, etc., to be used in specific applications. For instance, rectangular and circular shape horn antennas together with ridge guide horn antennas are reported in the literature [18-20]. Simple structures of these antennas are shown in Figure 1.3. Despite their advantages, the integration of such antennas with electronic systems used for specific applications can become a challenging task. For example, because of their non-planar structure horn antennas are not suitable for small handheld devices.

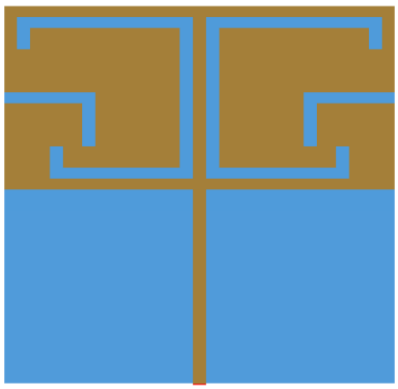

Figure 1.2 Structure of a printed monopole antenna

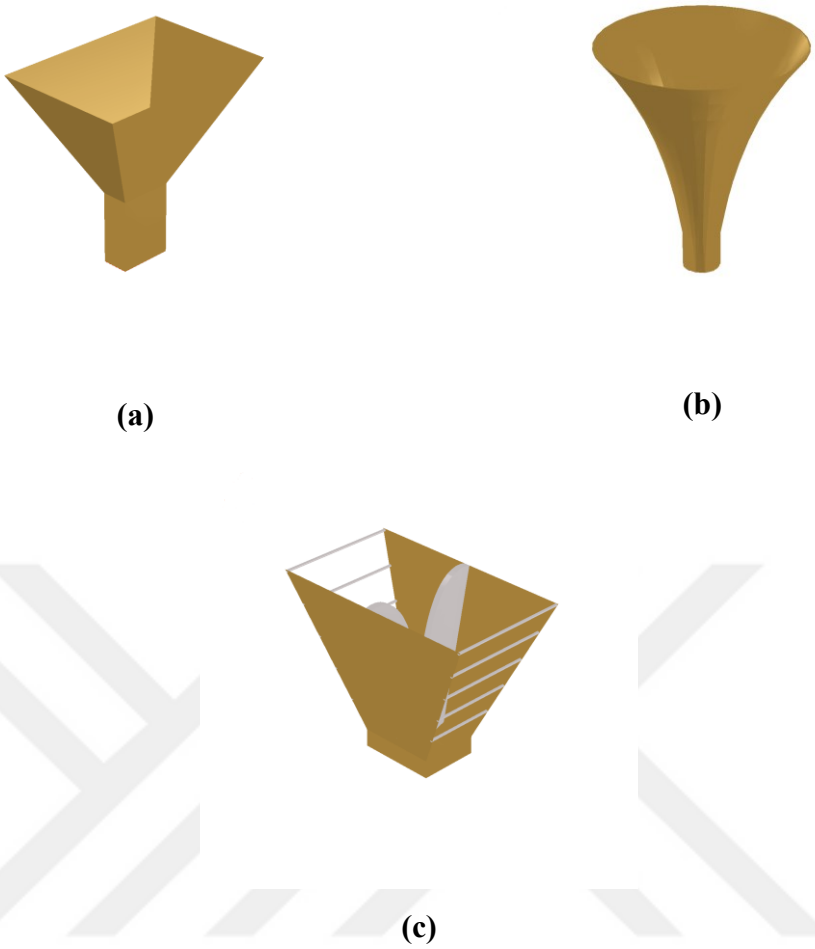

Figure 1.3 Structures of (a) Rectangular shape, (b) circular shape and, (c) double ridge guide horn antennas

As discussed above, proper selection of an antenna for UWB systems is a challenging task, because every antenna type offers certain pros and cons in terms of their radiation characteristics, design complexity, ease of implementation and cost. There are several studies in the literature which extensively investigate the performance metrics, design procedures and implementation costs of UWB antennas [21-23]. In these works, in addition to printed monopole patch antennas and horn antennas, wide-slot patch antennas, dielectric resonator antennas, and metamaterial structure antennas are reported. Among these antennas, wide-slot patch antennas are preferred for handset devices and phased array applications because of their compact sizes, planar structure and stable radiation patterns at high frequencies. Dielectric resonator antennas, on the other hand, can achieve band notch characteristics to reject signals at certain frequencies, which reduces interferences at these frequencies. Dielectric resonator antennas can also be designed to have compact sizes, and because of these properties they are often preferred

for communication applications where reducing interferences to other protocols such as WiMAX is critical [24]. Metamaterials possess unique properties such as negative permittivity and permeability, which enables metamaterial-based antennas to be used in a variety of different applications. For example, conformal antennas can be designed with metamaterials so that they can be used for wearable electronics, automotive radar or avionics, which require antennas to be flexible while maintaining the radiation characteristics [25].

Vivaldi antennas are another type of antenna that can operate in a wide frequency band. Vivaldi antennas are two-dimensional (2D) planar antennas, and they have end fire radiation characteristics. These properties make Vivaldi antennas a very good candidate to be used in several types of UWB systems including communication systems [26], radars [27], and satellites [28]. In the next chapter, Vivaldi antennas are introduced and explained in more detail. Also, the design methodology of a microstrip fed wideband Vivaldi antenna and its bandwidth optimization are explained. In addition, obtained results are given in the next chapter. In the third chapter, several performance enhancement techniques for Vivaldi antennas found in the literature, such as balun feed structure, corrugation and parasitic patch, are investigated and implemented on the antenna. The merit of these performance enhancement techniques are discussed based on simulation results presented in the third chapter. Finally, in the conclusions chapter, observations and deductions held in this thesis are briefly explained, possible future work based on this thesis and its societal impacts are discussed.

Chapter 2

Design of a microstrip fed ultra-wideband Vivaldi antenna and its bandwidth optimization

First introduced by P. J. Gibson in 1979, Vivaldi antennas are a type of aperiodic, continuously scaled travelling wave antenna [29]. A Vivaldi antenna consists of a radiating conductor on the top, a microstrip feed at the bottom, and a substrate between them. The radiation in Vivaldi antennas is achieved by a microstrip to slot line transition that occurs between the microstrip feed and the conductor plane. An electromagnetic wave travels through the linear slot while the separation between the conducting elements is gradually increased with an exponential taper profile. As the separation between the conductors increases, they are no longer able to confine the electromagnetic wave and the wave is radiated into free space. Due to their profile, Vivaldi antennas are also known as exponentially tapered slot antennas (ETSA). In Figure 2.1, a Vivaldi antenna with an exponentially tapered slot is shown from top and bottom views.

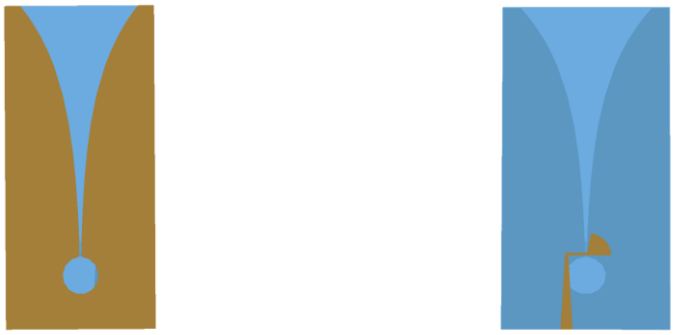

(a) **(b)**

Figure 2.1 (a) Top and, (b) bottom views of a Vivaldi antenna

The exponentially tapered profile of a Vivaldi antenna presented in [29] is expressed by Equation 2.1

$$Y = \pm A \exp(BX) \tag{2.1}$$

where X and Y represent coordinates of a point on the taper edges with respect to the origin placed at the radiator feed. A and B, on the other hand, represent the separation between the radiators at the start point of the exponential profile and the opening rate of the profile respectively. The unit of A is in mm, whereas the opening rate B is unitless. For the Vivaldi antenna presented in [29], A and B are 0.125 mm and 0.052, respectively. The separation between the conductors on the top is comparable to the wavelength of the signal that is being transmitted and because of the gradually increasing separation, from different parts of the Vivaldi waves at different frequencies radiate. However, along the aperture, the size of the radiating part becomes constant with frequency since radiated waves are no longer guided by the exponential flares. Thanks to their special structure, Vivaldi antennas theoretically have infinite bandwidth, which is limited by the lower cutoff frequency [30]. The reason for this is that the lower cut-off frequency is dependent on the total width of the antenna at the aperture. Generally, the width of a Vivaldi antenna should be greater than a quarter of the wavelength at its lowest operating frequency. As it can be seen from Equation 2.2, there is an inverse relationship between the wavelength of a signal and its frequency

$$\lambda = \frac{c}{f} \tag{2.2}$$

where λ is the wavelength expressed in meters, c is the speed of light in free space, which is approximately equal to $3\text{x}10^8$ m/s and f is the frequency. Because of the relation between the lower cut-off frequency of a Vivaldi antenna and its total width, Vivaldi antennas are not able to radiate signals below a certain frequency unless they are designed in much larger sizes, which may not be possible due to size constraints.

In addition to possible physical limitations and necessity to predetermine the lowest cut-off frequency, there might be further conditions while designing a Vivaldi antenna. As mentioned above, the bandwidth of a Vivaldi antenna is theoretically infinite. However, in practice bandwidth of an antenna is limited by the transition from the transmission line to the slot line, since it is difficult to have a good impedance matching

over a wide bandwidth. Input impedance of a Vivaldi antenna is set by its feeding line and the other parts of the antenna that couple to the feeding line. To address the bandwidth limitation, there have been several design studies to enhance the performance of Vivaldi antennas. One of the widely known design is the Antipodal Vivaldi Antenna (AVA) introduced by E. Gazit in 1988 [31]. Unlike Gibson's Vivaldi antenna, exponentially tapered flares of AVA are placed at the opposite sides of the substrate. At the input port, a ground plane is placed on one side of the substrate. However, the ground plane does not extend to the antipodal flares. Due to this feeding mechanism, at the input port there is a microstrip line structure, but it transitions to a double-sided parallel strip line due to the discontinuity of the ground plane and symmetric structure of the antipodal flares. With this feeding mechanism, AVA can achieve impedance matching over a wider bandwidth. However, AVAs suffer from poor cross-polarization performance. To overcome this problem, another type of Vivaldi antennas, called Balanced Antipodal Vivaldi Antenna (BAVA), was proposed by Langley et. al. in 1993 [32]. BAVA consists of two substrate layers and three exponentially tapered copper layers. Two of the copper layers lie at the top and bottom surfaces of the two substrates, while the third copper layer is located in between the substrates. In Figure 2.2, the structures of AVA and BAVA are shown. BAVA can overcome the impedance matching problem of the feed in Vivaldi antennas, and the poor cross-polarization problem of the AVA while achieving great bandwidths. However, they are costlier and harder to design compared to the other Vivaldis.

In the thesis, we focus on coplanar exponentially tapered slot conventional Vivaldi antenna, due to its relatively simpler design compared to other types of Vivaldi antennas. The main and initial objective is to design a Vivaldi antenna that can operate in the frequency range spanning from 2.4 GHz to 10.1 GHz, where the antenna is compatible with communication standards in the 2.4 GHz Industrial, Scientific and Medical (ISM) band while also supporting UWB communications in the 3.6 to 10.1 GHz band. To design the antenna, a powerful three dimensional (3D) electromagnetic simulation tool is used. After obtaining an initial design, performance enhancement techniques, which are discussed in the following chapters are implemented on the antenna.

2.1 Design of a microstrip fed Vivaldi antenna

There are several studies in the literature which investigate design parameters of Vivaldi antennas [33-34]. The geometrical size of a Vivaldi antenna is expressed in terms

of its operating wavelength, and thus the operating frequency. It has been shown that the minimum operating frequency of a Vivaldi antenna is inversely proportional to its total length and to the width of its aperture [34].

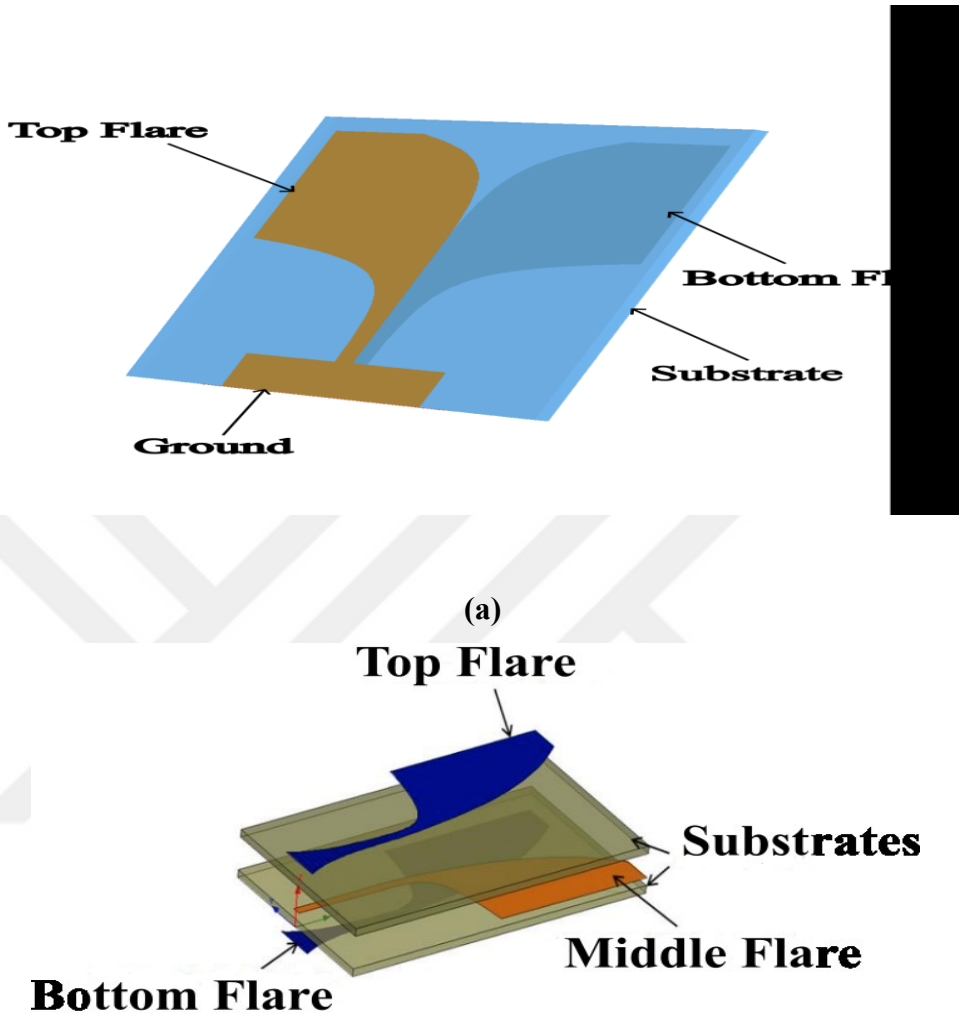

Figure 2.2 Structures of (a) Vivaldi antenna, (b) AVA and, (c) BAVA [35]

In theory, the maximum and minimum widths of a Vivaldi antenna aperture, i.e. w_{max} and w_{min} can be calculated as in Equations 2.3 and 2.4, respectively,

$$w_{max} = \frac{c}{2f_{min}\sqrt{\varepsilon_r}} \tag{2.3}$$

$$w_{min} = \frac{c}{f_c\sqrt{\varepsilon_r}} \tag{2.4}$$

where c is the speed of light, f_{min} is the lower cutoff frequency of the antenna, and ε_r is the dielectric constant of the substrate. Also, f_c is the center frequency of the antenna. For

the design, FR4 substrate with a dielectric constant (ε_r) equal to 4.4 was selected. Using Equations 2.3 and 2.4 with the selected FR4 substrate, a Vivaldi antenna that can operate in the UWB frequency regime between 3.6 GHz and 10.1 GHz was designed and its parameters were optimized with simulations [36]. The structure of the Vivaldi antenna and its geometrical parameters are shown in Figure 2.3 and the values of the parameters are given in Table 2.1. The parameters summarized in the table are named in coherence with the ones shown in Figure 2.3. In the table, W_{sub} is the width of the substrate, which is equal to the maximum width of the aperture calculated with Equation 2.3. The thickness of the FR4 substrate, *subh*, is 1.53 mm, and parameter a is the width of the linear slot measured from the center of the antenna. It has an important effect on the impedance of

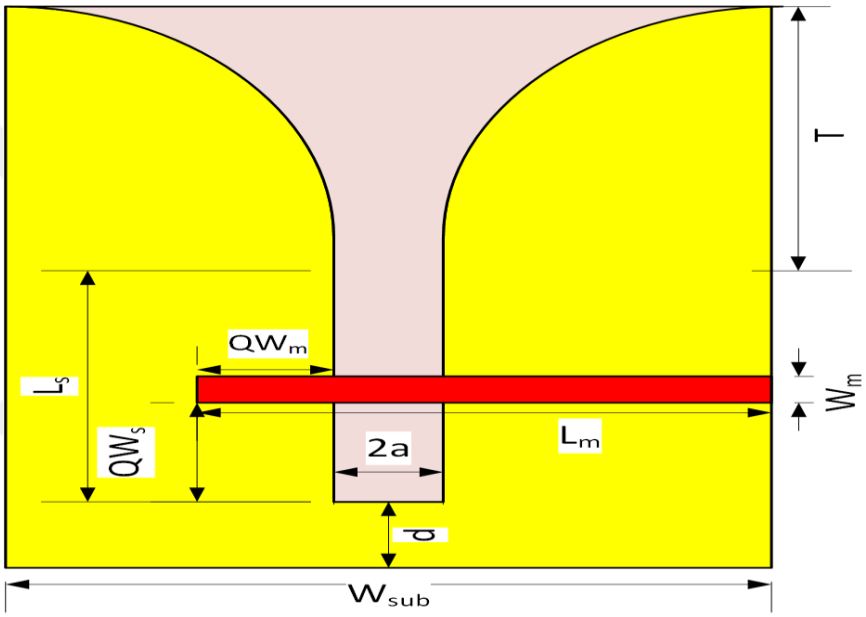

Figure 2.3 Structure of the designed Vivaldi antenna and its geometrical parameters

Table 2.1 Antenna Parameters

Parameter	**Dimension (mm)**	**Parameter**	**Dimension (mm)**
a	0.5	L_s	11
T	48	***d***	1
W_{sub}	60	W_m	3
QW_s	4	QW_m	4
subh	1.53	L_m	$QW_m+2a+W_{sub}/2$

the conducting plane, and its value is optimized to be 0.5 mm. The length of the linear slot is represented by L_s and its value is equal to 11 mm, whereas the length of the exponentially tapered flare is 48 mm, and it is represented by T. The exponential tapering of the flare is formulated by Equation 2.5,

$$y = C_1 e^{rx} + C_2 \tag{2.5}$$

where r is the opening rate of the exponential curve. C_1 and C_2, on the other hand, are the parameters related to the start and end points of the flare. If the flare starts from the point P1(x_1,y_1) and ends at the point P2(x_2,y_2), than C_1 and C_2 are found as follows.

$$C_1 = \frac{y_2 - y_1}{e^{rx_2} - e^{rx_1}} \tag{2.6}$$

$$C_2 = \frac{y_1 e^{rx_2} - y_2 e^{rx_1}}{e^{rx_2} - e^{rx_1}} \tag{2.7}$$

As seen in the figure and given in the table, in the designed antenna the linear slot starts with an offset d of 1 mm from the backwall of the antenna. In a design, the width of the microstrip line, W_m, should be chosen in such a way that the characteristic impedance of the microstrip is equal to 50 Ω. For a given characteristic impedance Z_0 and dielectric constant ε_r, the width of a thin microstrip line, W, can be calculated with Equation 2.8 [37]

$$\frac{W}{subh} = \begin{cases} \frac{8e^A}{e^{2A}} - 2, & for \frac{W}{subh} < 2 \\ \frac{2}{\pi}\left[B - 1 - \ln(2B-1) + \frac{\varepsilon_r - 1}{2\varepsilon_r}\left\{\ln(B-1) + 0.39 - \frac{0.61}{\varepsilon_r}\right\}\right], & for \frac{W}{subh} > 2 \end{cases} \tag{2.8}$$

where the parameters A and B can be found by Equations 2.9 and 2.10,

$$A = \frac{Z_0}{60}\sqrt{\frac{\varepsilon_r + 1}{2}} + \frac{\varepsilon_r - 1}{\varepsilon_r + 1}\left(0.23 + \frac{0.11}{\varepsilon_r}\right) \tag{2.9}$$

$$B = \frac{377\pi}{2Z_0\sqrt{\varepsilon_r}} \tag{2.10}$$

Using the formula, the width of the microstrip line having 50 Ω characteristic impedance on a FR4 substrate with 1.53 mm thickness and a dielectric constant of 4.4 is calculated as 3 mm. Moreover, in the figure and the table, the parameters QW_m and QW_s represent the longitudinal and latitudinal displacements of the microstrip feed with respect

to the linear slot. These parameters were initially chosen to be equal to the quarter wavelength inside the substrate at the center frequency and were later optimized. The last parameter, L_m, on the other hand, represents the total length of the microstrip line.

2.2 Simulation results

After obtaining the initial design as explained in Chapter 2.1, the parameters were optimized using a 3D electromagnetic simulation tool. The optimized parameters are summarized in Table 2.1. In the simulations, changes in resonance behavior, i.e. the return loss (or S11 parameter), realized gain and radiation pattern of the antenna with frequency were investigated. In Figure 2.4(a), it is seen that the antenna has a -10 dB bandwidth, i.e. the return loss or S11 parameter magnitude is less than or equal to -10 dB, over the frequency band from 3.1 to 13.6 GHz. Although the magnitude of the S11 parameter exceeds -10 dB around the frequencies 3.9, 7.8, 9.3 and 10.6 GHz, these excesses are negligibly small. S11 magnitude, |S11|, calculated at these frequencies are -9.2 dB, -9.5 dB, -9.7 dB and -9.3 dB, respectively. Furthermore, Figure 2.4(b) shows that the realized gain of the antenna over the frequency band from 3.1 to 13.6 GHz varies between 0.8 dBi and 5.5 dBi. Another important parameter of the antenna, which is its radiation pattern, was also analyzed and as it can be seen from Figure 2.4(c), the antenna has end-fire radiation characteristics at 5 GHz, which is desired for Vivaldi antennas.

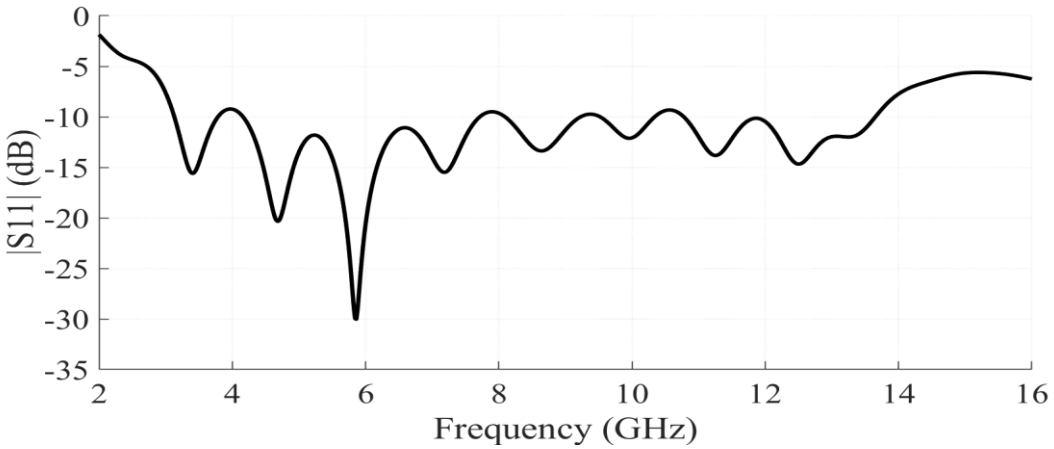

(a)

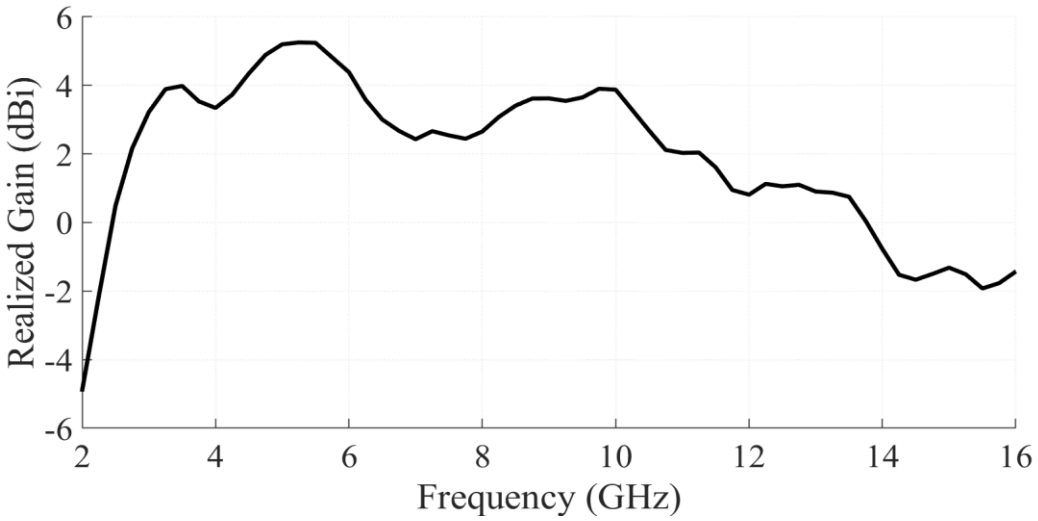

(b)

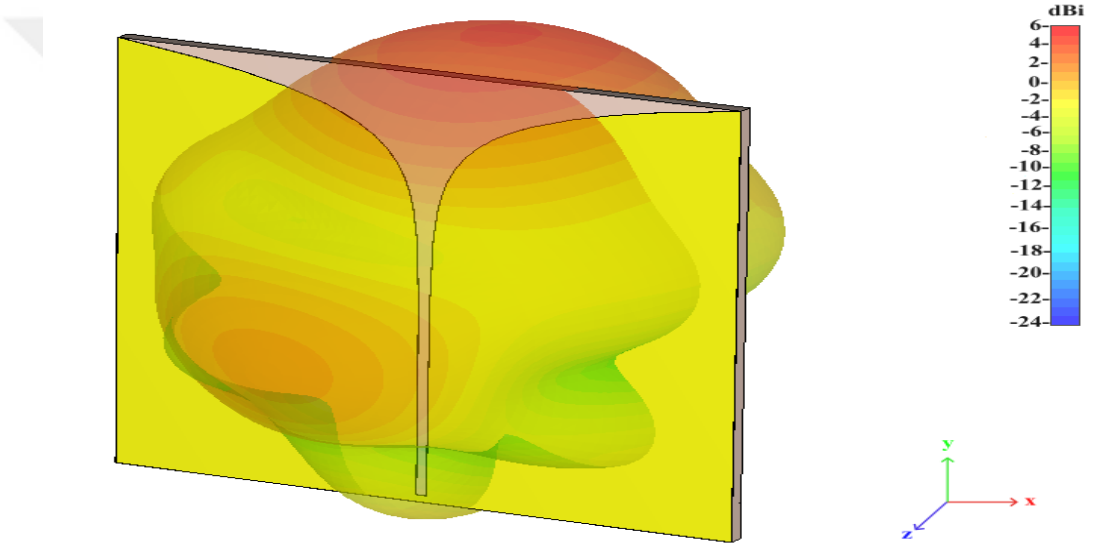

(c)

Figure 2.4 (a) Return loss, (b) realized gain and, (c) radiation pattern at 5 GHz of the optimized Vivaldi antenna calculated in the simulations**.**

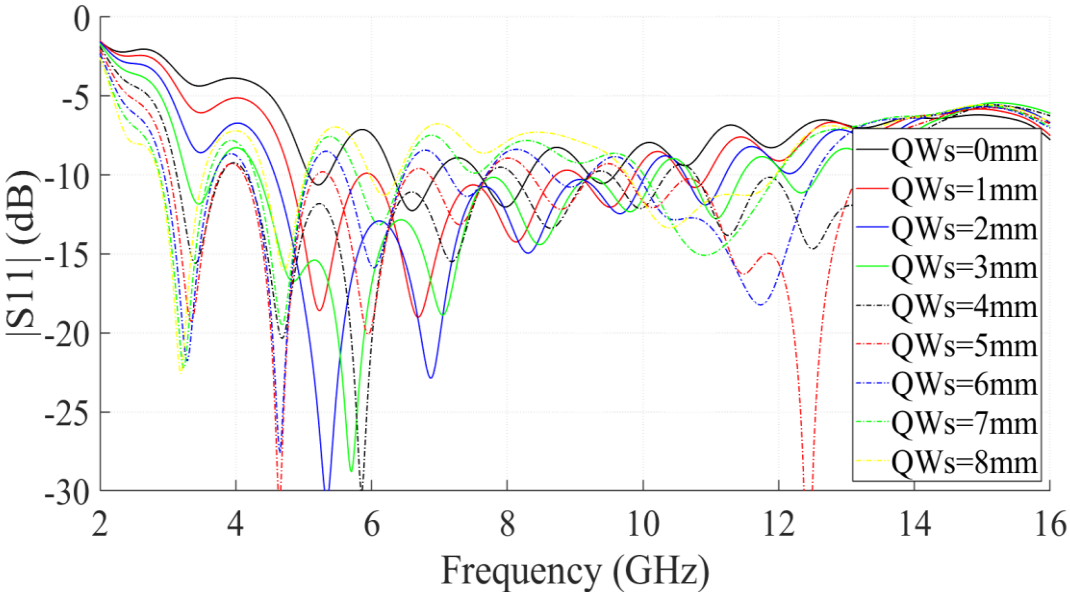

(a)

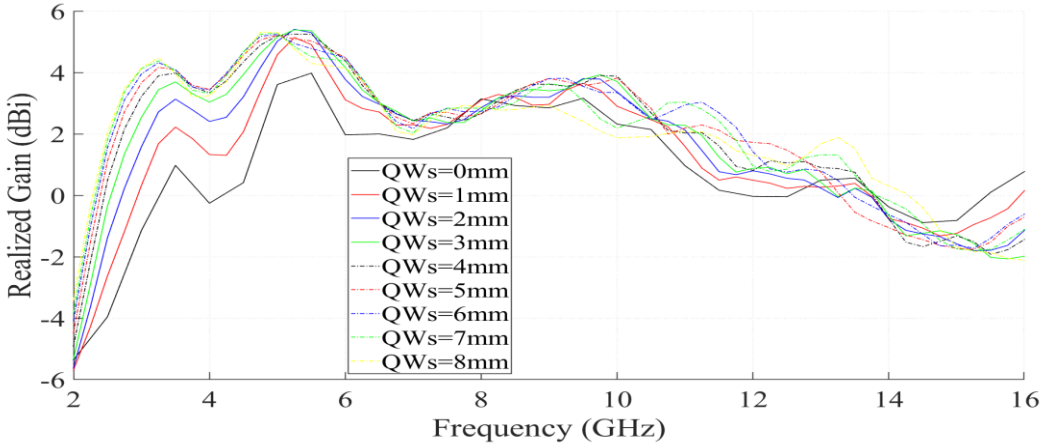

(b)

Figure 2.5 (a) Return loss and (b) realized gain changes of the designed antenna with frequency calculated in the simulations over the band between 2 and 16 GHz for constant QW_m = 4 mm exceed length and different QW_s distances

Above, it was discussed that the feeding mechanism is one of the most important factors affecting the performance of Vivaldi antennas. For this reason, after the initial design of the antenna was obtained and its parameters were optimized, a parametric sweep on the microstrip feed line was carried out. In this analysis, the feeding network parameters QW_s and QW_m were varied and the changes in the antenna's S11 parameters and realized gain over the frequencies spanning from 2 GHz to 16 GHz were observed.

First, simulations were done as the exceed length of the microstrip measured from the linear slot (QW_m) was kept constant at 4 mm, while the latitudinal displacement (QW_s)

of the strip line was incremented from 0 to 8 mm in 1 mm steps. In other words, simulations were done for the antenna while keeping the total length of the microstrip feed constant and moving it along the linear slot. S11 parameter magnitude and realized gain changes of the antenna calculated in the simulations are shown in Figure 2.5. From Figure 2.5(a), it is seen that as the parameter *QWs* is incremented from 0 mm until 5 mm, the lower cutoff frequency of antenna shifts towards lower frequencies while the higher cutoff frequency shifts towards higher frequencies, resulting in an increase in the bandwidth. However, if the latitudinal displacement is further increased up to 7 mm, both lower cutoff and higher cutoff frequencies shift towards lower frequencies resulting in an almost constant bandwidth. Furthermore, in Figure 2.5(b), it is seen that the realized gain of the antenna improves as QW_s is increased. The changes in the lower and higher cutoff frequencies, and the total bandwidth of the antenna versus parameter QW_s are represented in Figure 2.6.

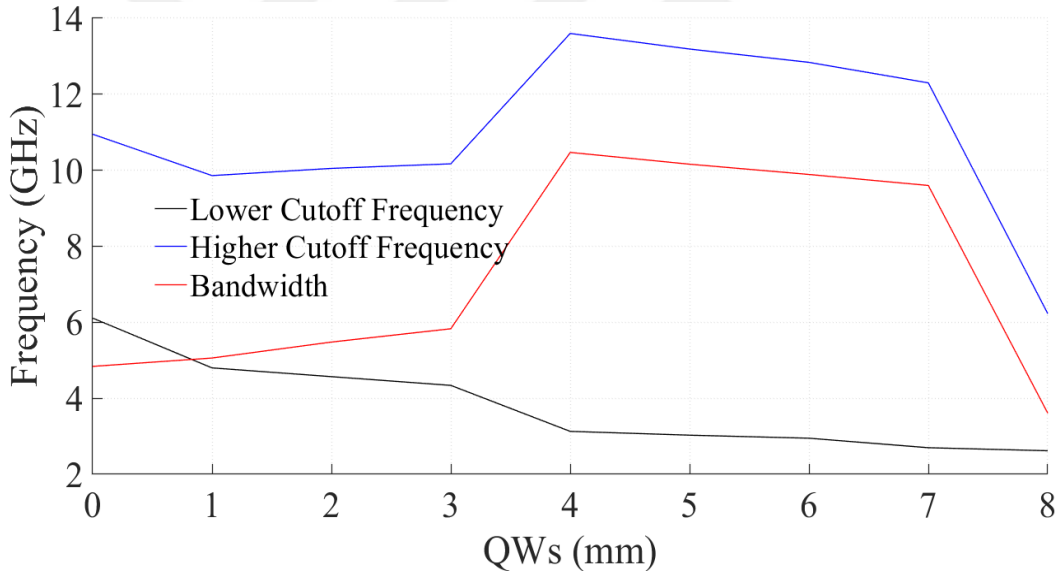

Figure 2.6 Lower and upper cutoff frequency shifts and bandwidth change of the antenna for constant QW_m = 4 mm exceed length and different QW_s distances

Next, the simulations were repeated for the antenna having a constant longitudinal displacement, QW_s, equals to 4 mm and the exceed length of the microstrip, QW_m, incremented from 0 mm to 8 mm with 1 mm steps. Changes in the antennas S11 parameters and realized gain over the frequencies ranging from 2 GHz to 16 GHz with exceed length of the microstrip, QW_m, are shown in Figure 2.7. Also, the changes in the cutoff frequencies and the bandwidth of the antenna are represented in Figure 2.8. In the

figures, it is seen that the lower cutoff frequency of the antenna shifts towards lower frequencies and the higher cutoff frequency shifts towards higher frequencies as QW_m is increased from 0 mm to 4 mm. However, as the parameter is further incremented, the lower cutoff frequency mostly remains the same while the higher cutoff frequency decreases, resulting in a reduced bandwidth. On the other hand, realized gain of the antenna considerably improves with the increase in QW_m parameter at low frequencies, i.e. between 2 GHz and 5 GHz, while there is no constant increase or decrease at high frequencies.

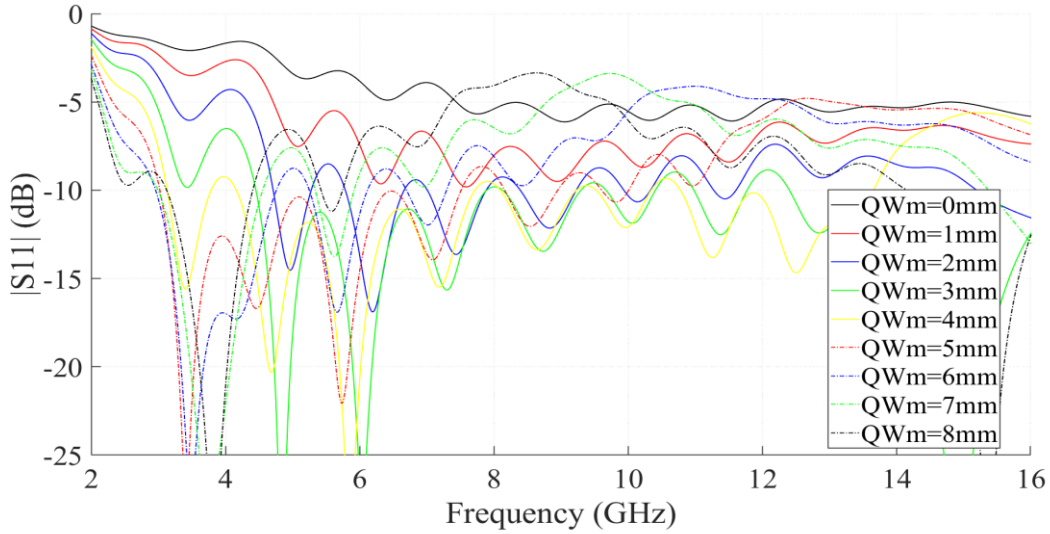

(a)

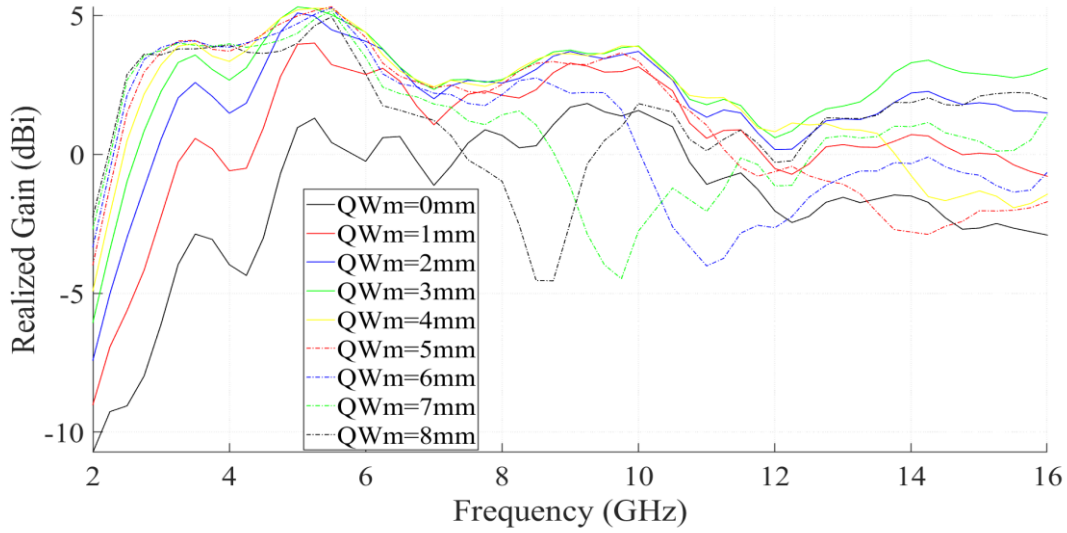

(b)

Figure 2.7 (a) Return loss and (b) realized gain changes of the designed antenna with frequency calculated in the simulations over the band between 2 and 16 GHz for constant QW_s = 4 mm distance and different QW_m exceed lengths

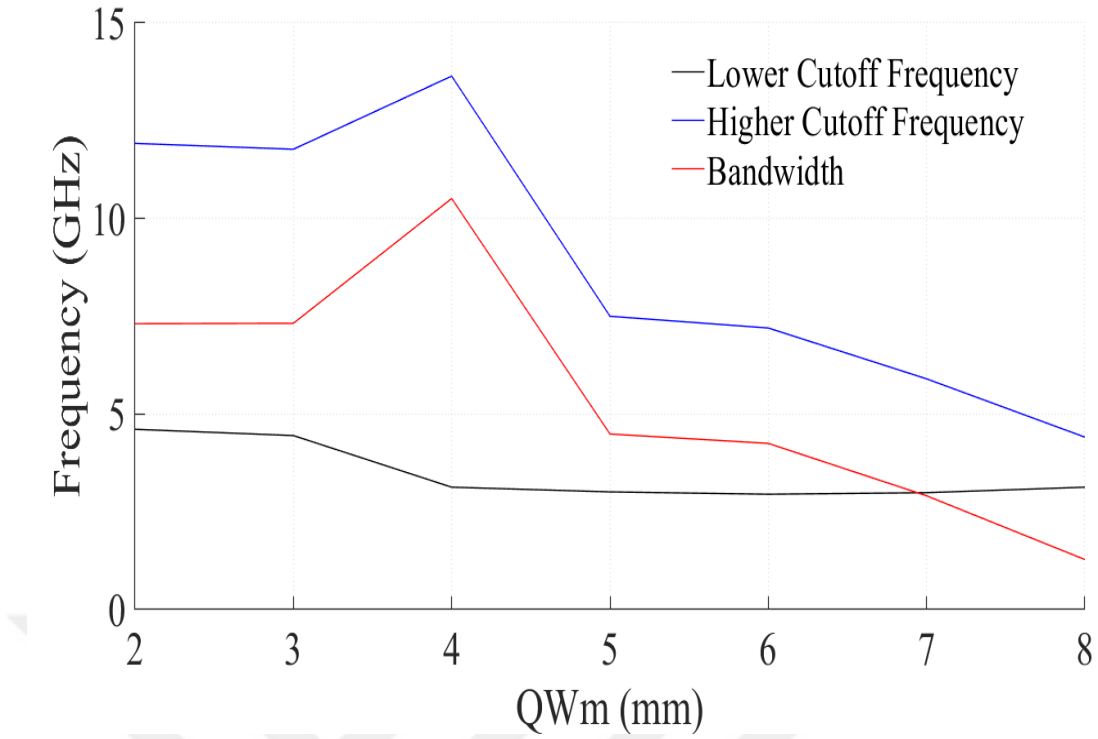

Figure 2.8 Lower and upper cutoff frequency shifts and bandwidth change of the antenna for constant QW_s = 4 mm exceed length and different QW_m distances

In the simulations discussed above, one of the parameters from QW_s and QW_m was kept equal to the optimized length of 4 mm while the other parameter was changed. To gain a deeper understanding of the effect of the microstrip line on the antenna performance, simulations were continued for the antenna with QW_s and QW_m parameter values different from the initial value of 4 mm. Figures 2.9, 2.10 and 2.11 show the changes in the S11 parameter magnitude and realized gain of the antenna for constant exceed lengths of the microstrip feed, QW_m, equal to 2 mm, 3 mm and 5 mm, respectively, where longitudinal displacement of the feed line, QW_s, is increased starting from 0 mm till 8 mm with 1 mm steps. From the figures, one can observe that as the parameters QW_s and QW_m are changed concurrently the bandwidth of the antenna shifts. Furthermore, while the shift in the bandwidth occurs, the realized gain of the antenna alters as well such that the changes in the antenna gain with parameters QW_s and QW_m follow a similar trend. The changes in the lower and higher cutoff frequency of the antenna and its total bandwidth with QW_s and QW_m parameters is better represented in Figure 2.12. The figure shows that one can in fact tune the operating bandwidth of the antenna within some limits while maintaining a similar realized gain profile by changing only the total length of the microstrip feed and its displacement along the linear slot.

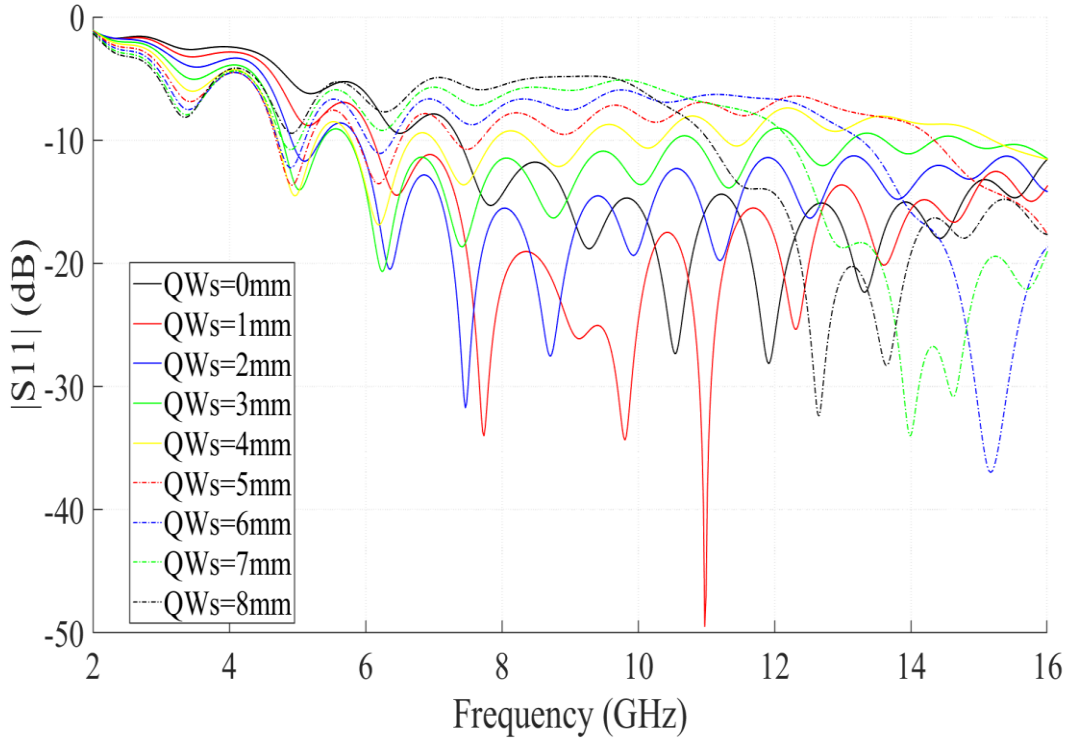

(a)

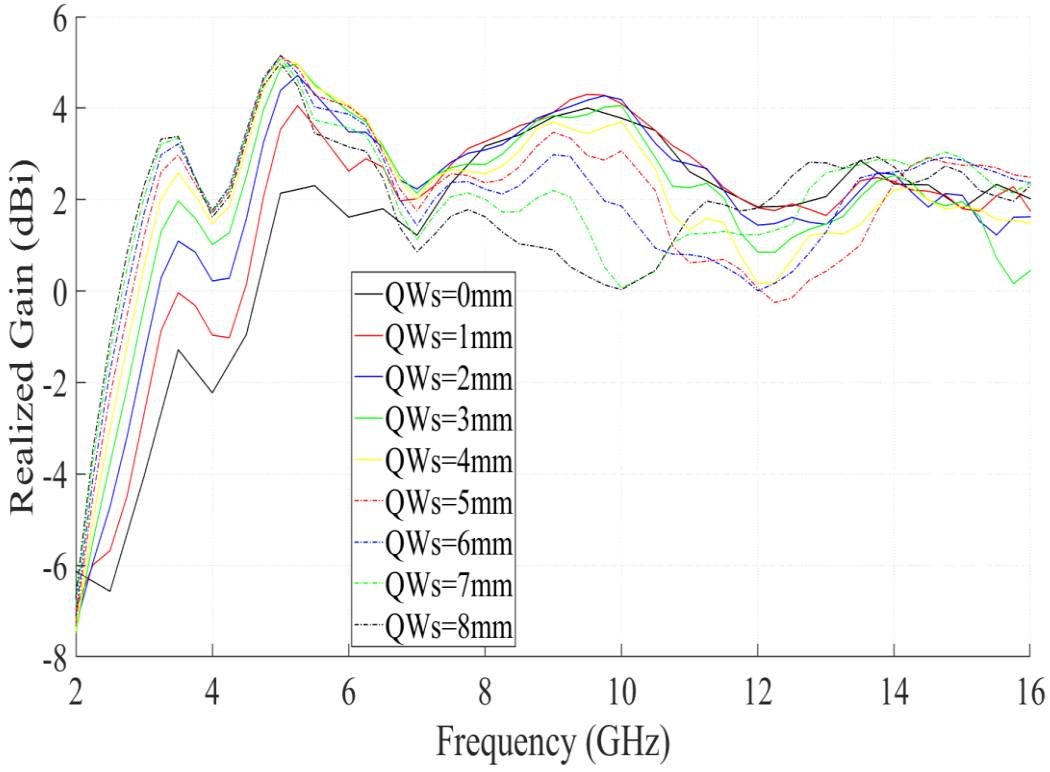

(b)

Figure 2.9 (a) Return loss and (b) realized gain changes of the designed antenna with frequency calculated in the simulations over the band between 2 and 16 GHz for constant QW_m = 2 mm exceed length and different QW_s distances

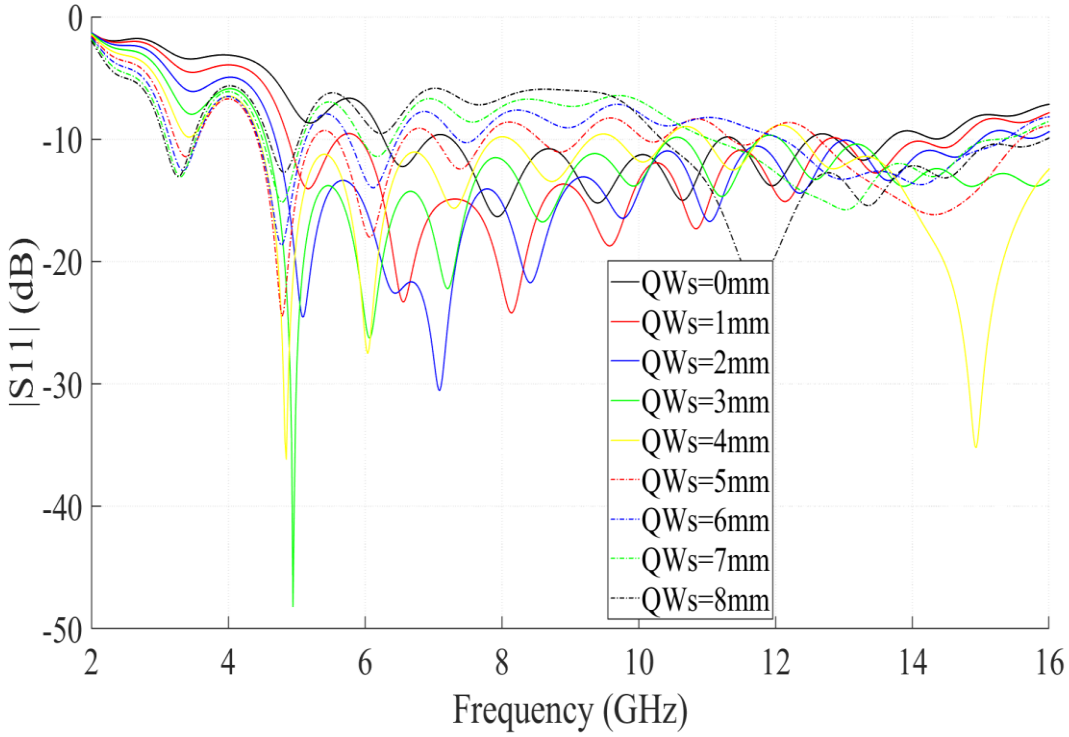

(a)

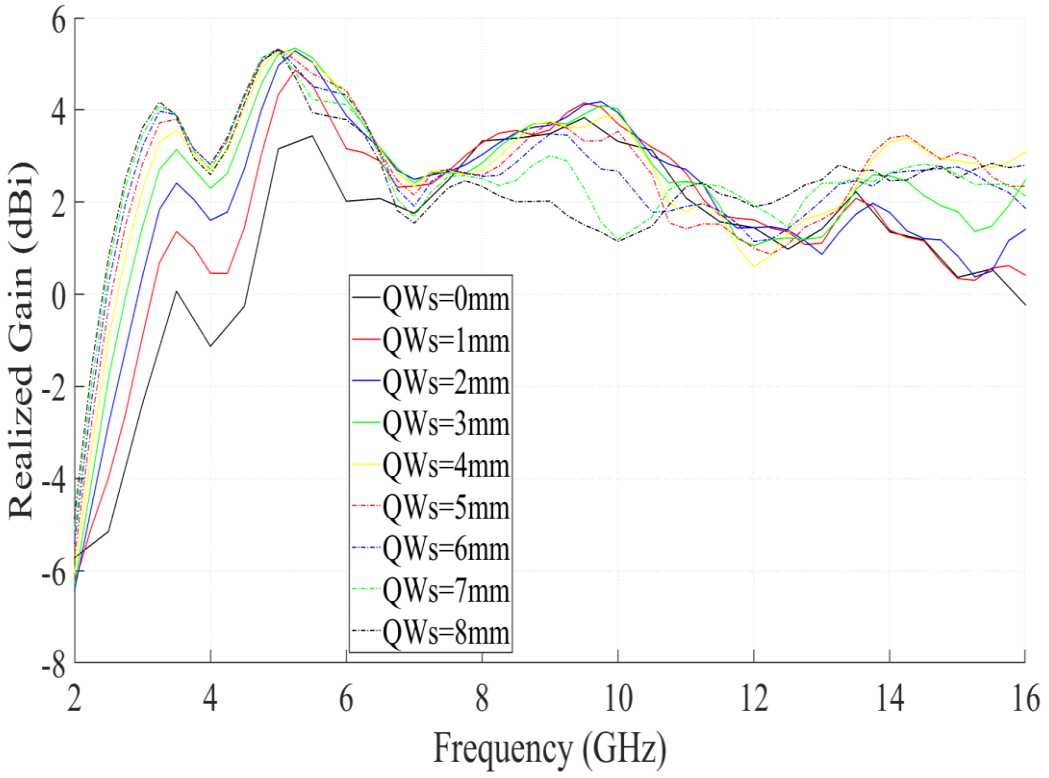

(b)

Figure 2.10 (a) Return loss and (b) realized gain changes of the designed antenna with frequency calculated in the simulations over the band between 2 and 16 GHz for constant QW_m = 3 mm exceed length and different QW_s distances

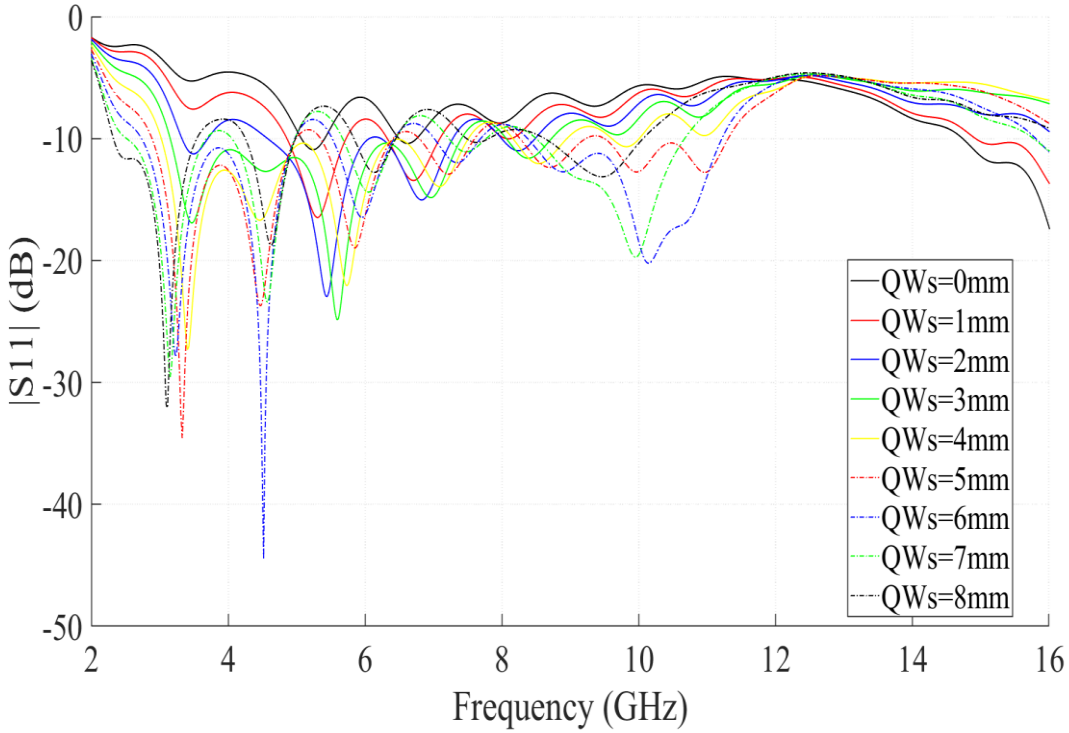

(a)

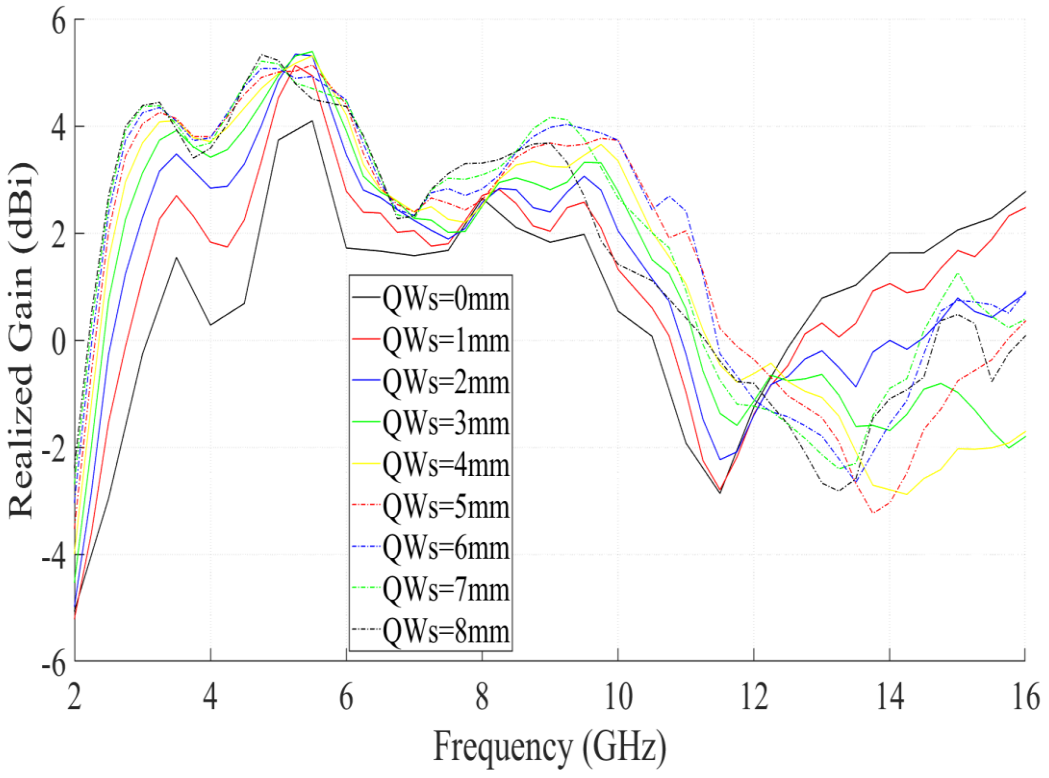

(b)

Figure 2.11 (a) Return loss and (b) realized gain changes of the designed antenna with frequency calculated in the simulations over the band between 2 and 16 GHz for constant QW_m = 5 mm exceed length and different QW_s distances

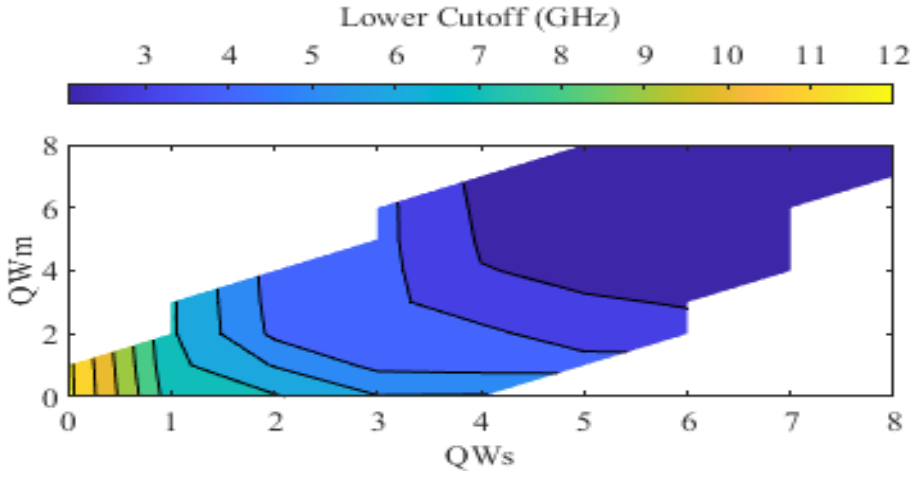

(a)

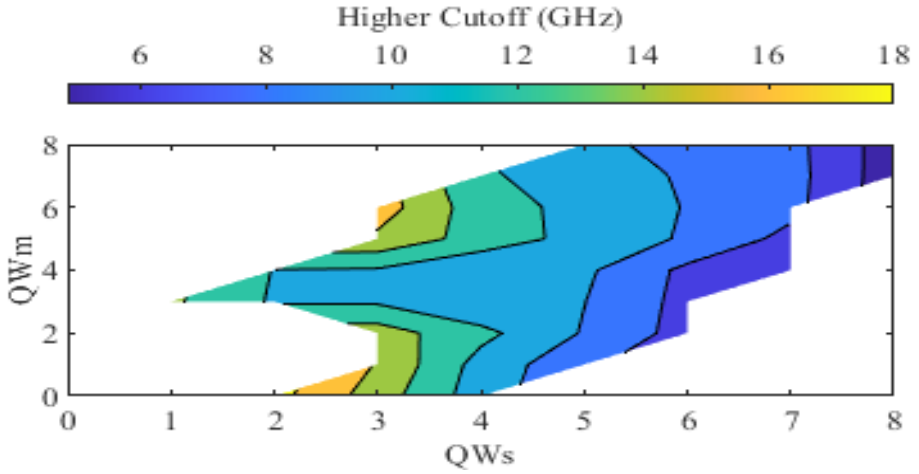

(b)

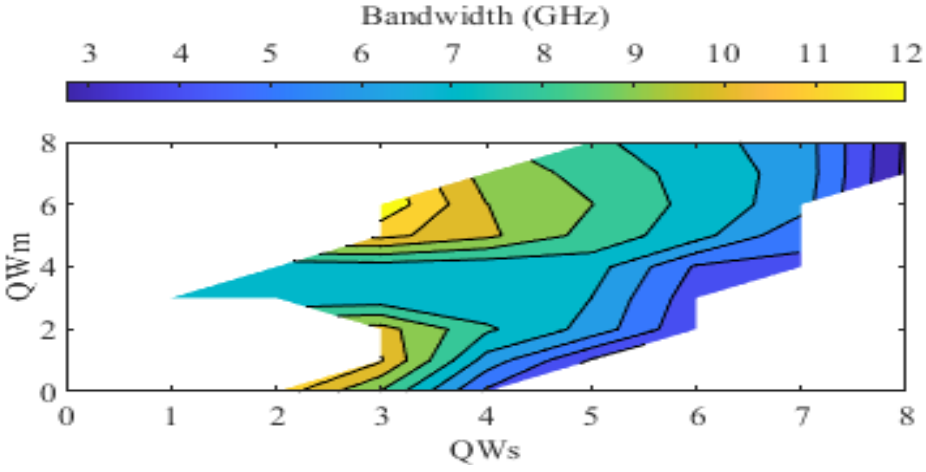

(c)

Figure 2.12 (a) Lower cutoff frequency, (b) higher cutoff frequency and, (c) bandwidth changes of the designed antenna for different QW_s distances and QW_m exceed lengths

Chapter 3

Performance enhancement techniques applied for the designed Vivaldi antenna

In the previous chapter, it was shown that realizing the design of a Vivaldi antenna operating at UWB frequencies (3.6 to 10.1 GHz) is possible with a simple architecture that consists of

- a conducting metal surface with a linear slot and two exponentially tapered flares as shown in Figure 2.3,
- a substrate material,
- and a microstrip line.

However, this design has low a gain and it is not able to maintain the end-fire radiation pattern over a wide frequency range. In addition, the antenna should be scaled down to operate at lower frequencies, which results in the designed antenna side lengths to be quite larger than few centimeters (see table 2.1 for the geometric parameters of the designed antenna).

In the literature, there are various studies that address the limitations of Vivaldi antennas and propose methods for miniaturization of the size of the antenna, improving the impedance matching over a wide band of frequencies, improving the directivity and gain of the antenna. For instance, resistive loading of the Vivaldi antenna is one of the methods in the literature, which is used for improving the impedance matching of Vivaldi antennas and can also serve as a miniaturization technique as discussed in [38-40]. On the other hand, the use of a dielectric director is one of the methods presented in the literature which is used to improve the directivity and gain of Vivaldi antennas [40-41]. Furthermore, to overcome the cross-polarization and beam tilt problems observed in the Vivaldi antennas, and to improve the gain, covering the antenna with a dielectric slab on both top and bottom surfaces is proposed in [42]. A detailed overview of these

enhancement methods along with other methods presented in the literature can be found in [43].

To improve the performance of the antenna designed in the previous chapter, we adopted three enhancement methods. The first method is to add a circular cavity in the radiating flares and terminating the microstrip feed with a radial stub. This method serves the purpose of improving the impedance matching of the antenna. The second method is to apply corrugations to the sides of the exponential flares, and this method serves the purpose of further improving the impedance matching of the antenna at lower frequencies, size miniaturization and gain improvement. The last method applied on the designed antenna is placing parasitic patch and lens structures, which further improves the gain of the Vivaldi antenna. In the remainder of this chapter, the methods applied, and changes made in the antenna structure are explained in detail.

3.1 Adding a circular cavity and radial stub termination to improve the feeding network and impedance matching

One of the methods, which has become a common practice in the design of Vivaldi antennas, is to add a circular cavity in the conducting metal surface located at the bottom of the linear slot [44-45]. The circular cavity, or slot, acts as an open circuit against the reflections from the linear slot and assists the electromagnetic coupling in the microstrip-to-slot line transition of the feeding mechanism. Another method accompanying to the circular cavity that improves the impedance matching of the feeding network is to terminate the microstrip feed with a radial stub [46]. The stub termination can be in different shapes, but usually a stub with a radial geometry is used. In [47], radial stub and circular stub terminated microstrips used as a feeding network for a Vivaldi antenna are investigated. Furthermore, in [48], effects of different parameters of the radial stub termination including longitudinal and latitudinal displacement of the stub and its offset angle are examined. From these studies, it is clearly seen that choosing a proper geometry for the feed network has a significant impact on the impedance matching of the antenna.

In Figure 3.1, the structure of a Vivaldi antenna with a circular cavity and a radial stub terminated microstrip feed is illustrated.

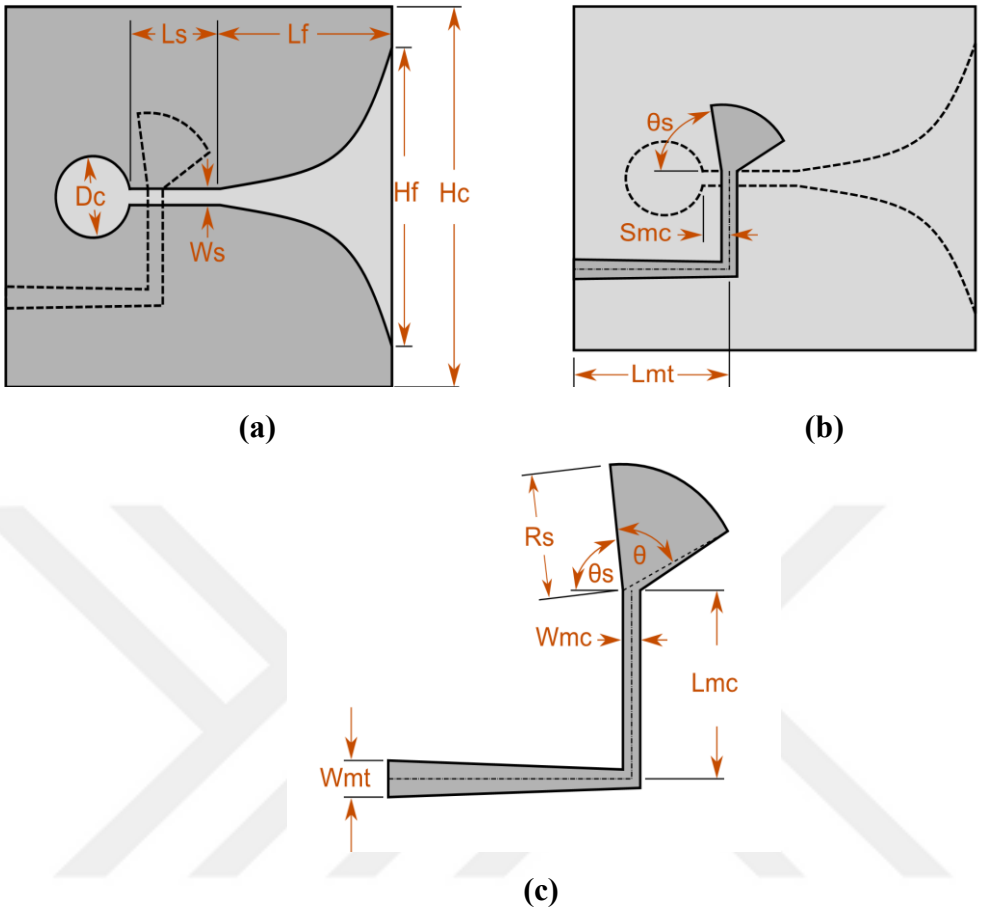

Figure 3.1 (a) Top view, (b) bottom view and, (c) microstrip feed structure of the Vivaldi antenna with its geometrical parameters

In the figure, parameters D_c and R_s represent the diameters of the circular cavity and the radial stub. Similarly, L_s, L_f, L_{mt} and L_{mc} stand for the lengths of the linear slot, exponential flare, tapered microstrip and the microstrip coupler, respectively. Widths of the linear slot, tapered microstrip and the microstrip coupler, on the other hand, are labeled with W_s, W_{mt} and W_{mc}, respectively. In addition, the parameter S_{mc} is the inset of the microstrip coupler measured from the start point of the linear slot. The angular parameters of the radial stub, i.e., the total angle of the stub and its start angle from the linear slot, are displayed by the parameters θ and θ_s, respectively. Moreover, in the figure the parameters H_f and H_c represent the widths of the aperture and the substrate, respectively.

3.1.1 Design and simulation results of the Vivaldi antenna with the circular cavity and radial stub terminated microstrip feed

As discussed above, a circular cavity is supposed to improve the impedance matching by reducing the reflections occurring from the linear slot in a Vivaldi antenna. In practice, the diameter of the circular cavity is often set to be equal to a sixth of the effective wavelength of the slot line at $2f_{min}$, where f_{min} is the minimum frequency at which the antenna operates. Relations between the diameter of the circular cavity, effective wavelength of the slot line and the minimum operating frequency of the antenna are given in Equations 3.1, 3.2 and 3.3. This value is chosen to avoid the circular cavity behaving like a short circuit at low frequencies in the operating band.

$$D_C \cong \frac{\lambda_{gs}}{6} \tag{3.1}$$

$$\lambda_{gs} \cong \frac{c}{2f_{min}\sqrt{\varepsilon_{eff}}} \tag{3.2}$$

$$\varepsilon_{eff} = \begin{cases} \frac{\varepsilon_{R+1}}{2} - \frac{\varepsilon_R - 1}{2}\left\{\frac{1}{\sqrt{1+12\left(\frac{H_{st}}{W_s}\right)}} + 0.04\left[1-\left(\frac{W_s}{H_{st}}\right)^2\right]\right\}, & for\ \frac{W_s}{H_{st}} < 1 \\ \frac{\varepsilon_{R+1}}{2} + \left[\frac{\varepsilon_R - 1}{2\sqrt{1+12\left(\frac{H_{st}}{W_s}\right)}}\right], & for\ \frac{W_s}{H_{st}} > 1 \end{cases} \tag{3.3}$$

In the equations above, λ_{gs} represents the effective wavelength of the slot line at $2f_{min}$, ε_{eff} represents the effective dielectric constant of the substrate at the slot line and ε_R is the real dielectric constant of the FR4 substrate. W_s and H_{st}, on the other hand, are the width of the slot line and height of the substrate, respectively. Similarly, the diameter of the radial stub is adjusted to be a sixth of the effective wavelength of the microstrip line at $2f_{min}$. Here, again f_{min} represents the minimum antenna operating frequency. Relations between the diameter of the radial stub, effective wavelength of the microstrip line and the minimum antenna operating frequency can again be found from Equations 3.1, 3.2 and 3.3 by plugging in the width of the microstrip coupler, W_{mc}, in the place of W_s.

In addition, to improve the impedance matching even further, a microstrip line with 50 Ω characteristic impedance at its input side and 100 Ω characteristic impedance at the

linear slot side is designed by using Equation 2.8. This type of feed networks are called baluns (balanced to unbalanced). Although their designs are more complicated compared to rectangular microstrips, baluns can improve the impedance matching over wide frequency bands [49]. Based on this and using Equations 2.3-2.7, a new Vivaldi antenna with circular cavity and radial stub terminated microstrip feed operating in the ultra-wide frequency band was designed, and its parameters were optimized. The structure of the antenna is as illustrated in Figure 3.1. The values of the geometrical parameters of the design are given in Table 3.1. In the table, the parameters are exactly the same with those used in the figure.

Table 3.1 Geometrical parameters of the antenna

Parameter	Dimension (mm)	Parameter	Dimension (mm)	Parameter	Dimension (mm)
D_c	10.11	H_c	108.45	W_{mc}	0.91
L_s	0.88	L_{mt}	22	L_{mc}	22
L_f	164	S_{mc}	0.43	R_s	6.75
W_s	0.75	θ_s	86	θ	80.6
H_f	90.7	W_{mt}	2.76	H_{st}	1.5

As for the previous designs, simulations were obtained for the antenna. The return loss and realized gain changes of the optimized antenna with frequency calculated in the simulations are shown in Figure 3.2. It is seen from the figure that this new design with the circular cavity, radial stub terminated balun feed structure has a -10 dB bandwidth ranging between frequencies 1.33 GHz and 10.1 GHz. Although this design has a narrower -10 dB bandwidth compared to its counterpart presented in the previous chapter, its main improvement is seen in its realized gain and directive radiation pattern. The previous design had an average realized gain of 2.75 dBi over its operating bandwidth, whereas this new design has an average realized gain of 6 dBi. This indicates that the improved design is able to maintain end-fire radiation characteristics over a wide bandwidth with significantly higher gain between the frequencies 3 and 7 GHz. The improvement in the radiation characteristics is clearly seen in Figure 3.3, which shows the far field radiation pattern of the antenna at 5 GHz. As it can be seen from the figure, the realized gain of the antenna at this frequency is 11.3 dBi, whereas this value was 5 dBi for the previous design (see Figure 2.4).

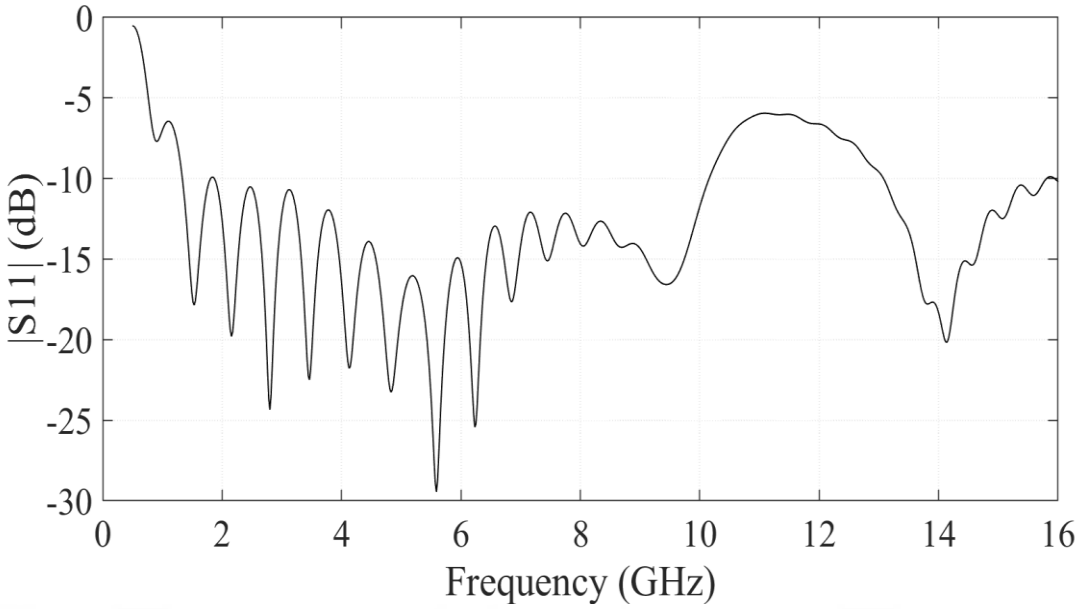

(a)

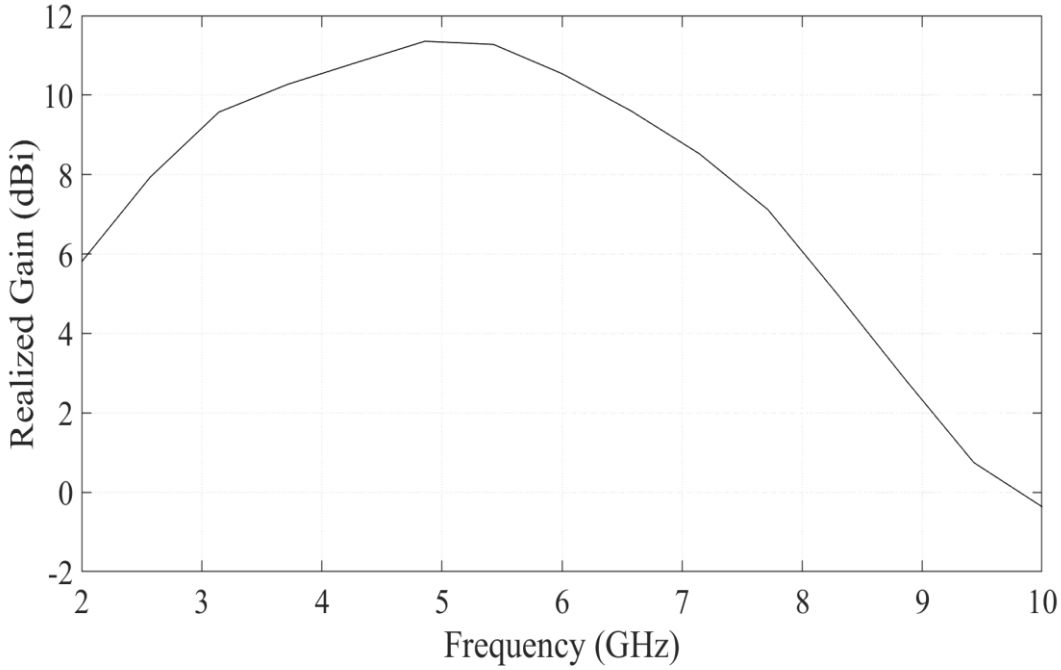

(b)

Figure 3.2 (a) Return loss and, (b) realized gain changes of the optimized antenna having the circular cavity and radial stub terminated microstrip feed calculated in the simulations

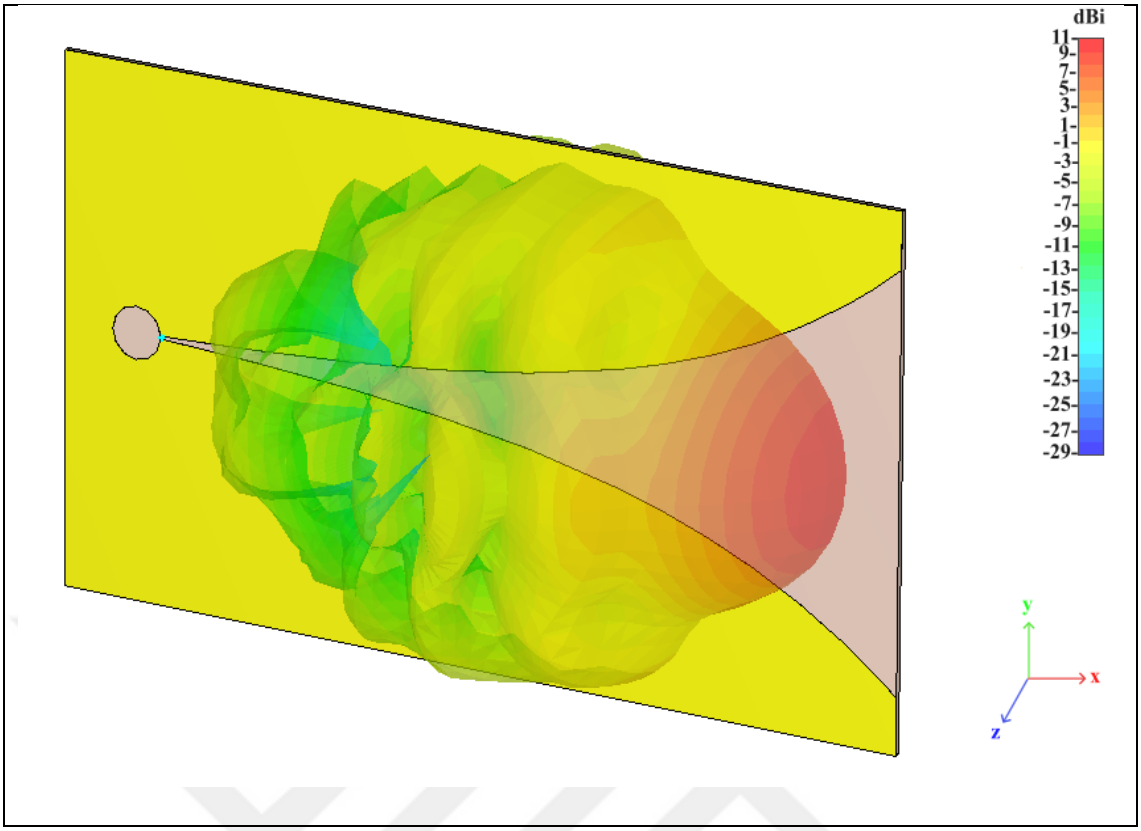

Figure 3.3 Far field pattern of the optimized antenna having the circular cavity and radial stub terminated microstrip feed at 5 GHz calculated in the simulations

3.2 Corrugation

Another method for improving the performance of Vivaldi antennas is to use corrugation. Corrugation is set by opening slots on the flares of the Vivaldi antenna, which are often evenly spaced, repetitive and have the same shape. Some of the corrugation types found in the literature are comb shaped corrugation, rectangular corrugation and sine wave corrugation [50-52]. These studies have shown that corrugating the flares of an antipodal Vivaldi antenna improves the antennas radiation pattern, enhances its gain and its impedance matching by minimizing the surface currents on the sides of the flares and reducing the reflections. However, as mentioned in [53], corrugation has been more commonly implemented on AVAs and BAVAs, but not on coplanar Vivaldi antennas. Among the different corrugation types, sine corrugation refers to opening a slot on the antennas flares whose profile is defined by a sinusoidal function. Due to its ease of implementation in the design phase, sine corrugation is adopted in this thesis. Furthermore, to the best of our knowledge, the effects of implementing a sine corrugation

on coplanar Vivaldi antennas with nonuniform amplitude and periodicity is investigated for the first time in the literature. In the following chapter, the effects of adding the sine wave corrugation on the designed antenna presented in Chapter 3.1 will be discussed.

3.2.1 Design and simulation results of the Vivaldi antenna with the circular cavity, radial stub terminated microstrip feed and sine corrugation

For the design of the antenna with the sine corrugation, the same geometrical parameters listed in Table 3.1 were used. Then, on the outer edges of the exponentially tapered flares, a sine corrugation was introduced whose profile is defined as

$$y = A \sin kx \tag{3.4}$$

where A is the amplitude of the sine function and k is a parameter related to the periodicity of the function in space. Also, x and y correspond to the coordinate axis values of a point that is on the edge. Relation between periodicity of the sine function, which is represented with T, and the parameter k is given in Equation 3.5.

$$T = \frac{2\pi}{k} \tag{3.5}$$

Top view of the structure of the Vivaldi antenna with sine corrugation is shown in Figure 3.4. In the figure, x and y axis are also pointed out so that the coordinate axis values of a point on the edge can be determined.

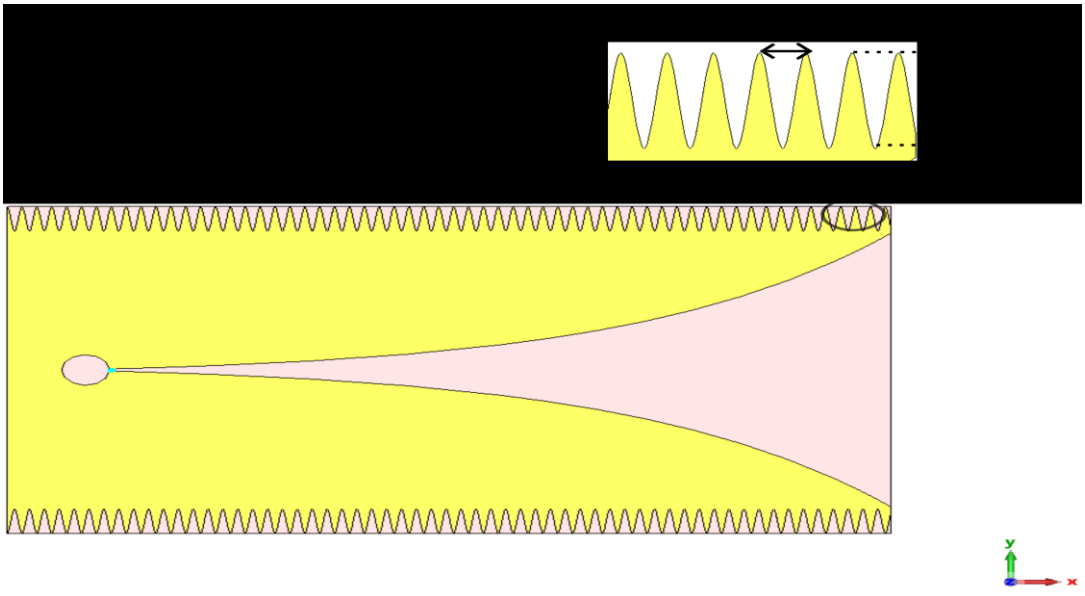

(a)

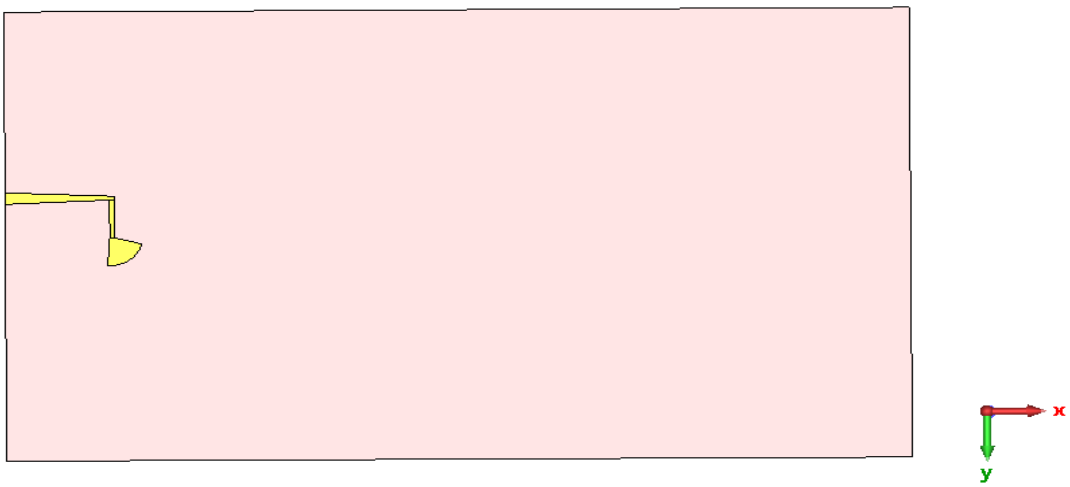

(b)

Figure 3.4 (a) Top and (b) bottom view of the structure of the Vivaldi antenna with a sine corrugation

Simulations and analysis were done for the designed antenna with the sine corrugation of various amplitudes and periods. The return loss and the realized gain changes of the antenna as a function of frequency for a sine corrugation with the constant period, T = 3.14 mm, k = 2 mm^{-1}, and different amplitudes varied between 1 mm and 4 mm are shown in Figure 3.5. It is seen from the figure that adding a sine wave corrugation to the antenna with the constant period, T = 3.14 mm, k = 2 mm^{-1}, does not affect the return loss significantly when its amplitude is small. However, when the amplitude A = 4 mm is reached, there is a considerable improvement in the return loss especially at low frequencies within the operating band. On the other hand, in Figure 3.5(b) one can see that the realized gain of the antenna increases differently for distinct sine amplitude values at various frequencies. The best improvement is observed between frequencies 4 GHz and 6.5 GHz for the amplitude of 3, whereas at higher frequencies starting from approximately 8 GHz, the only improvement over the non-corrugated model is observed for the amplitude of 1 mm.

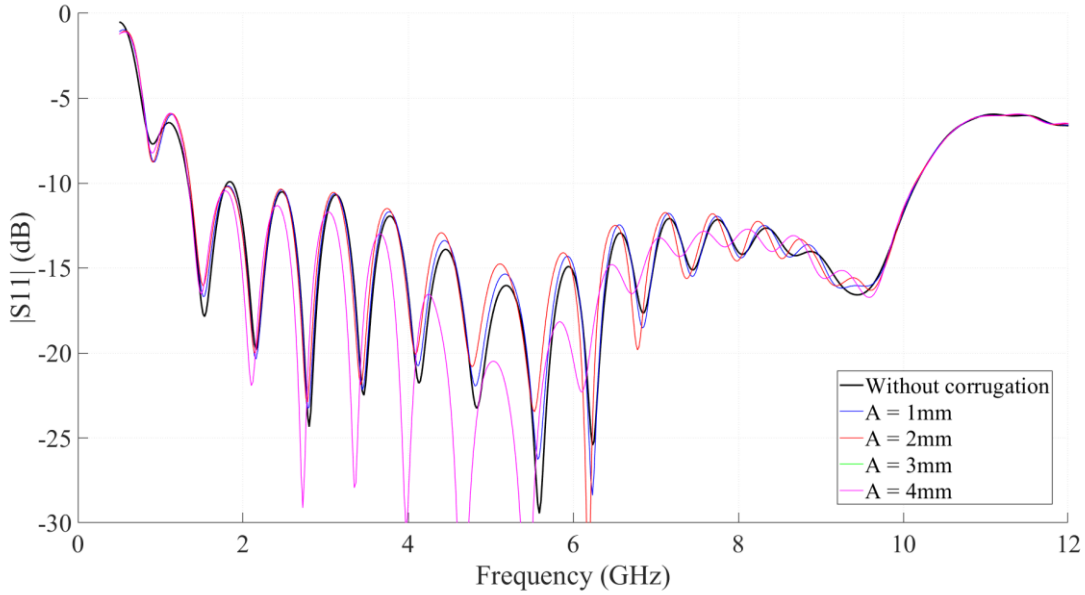

(a)

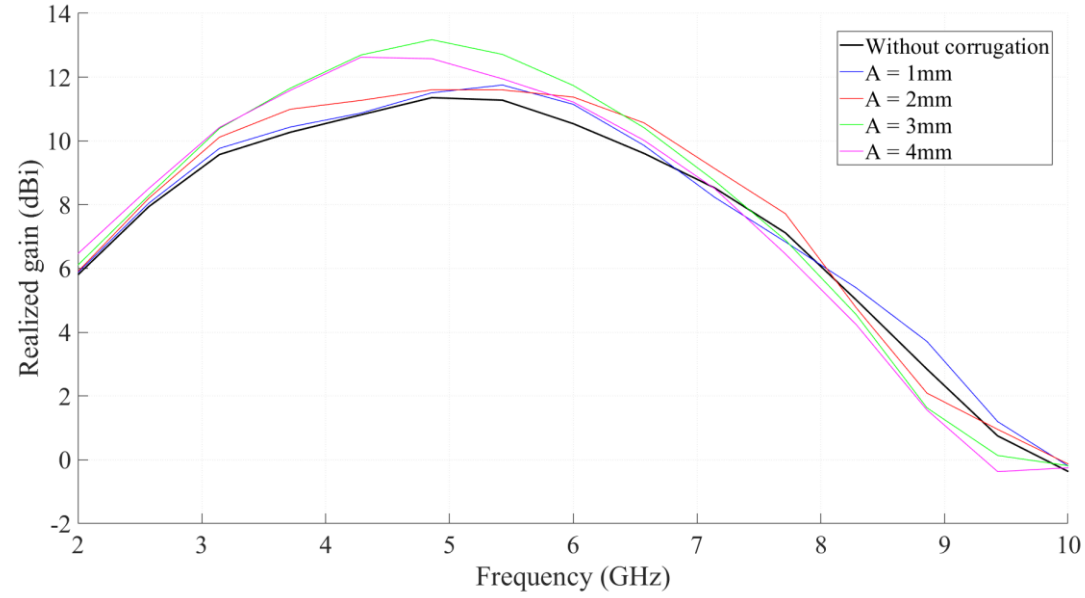

(b)

Figure 3.5 (a) Return loss and, (b) realized gain changes of the sine corrugated antenna with constant period, T = 3.14 mm, k = 2 mm^{-1}, and different amplitudes calculated in the simulations

Simulations were repeated for 3 mm constant amplitude of the corrugation, i.e. A = 3 mm, and different values of the period, such that the parameter k is varied between 1 mm^{-1} and 4 mm^{-1}. The results are shown in Figure 3.6. From the figure, it is seen that there is no significant degradation in the return loss when the period of the sine

corrugation is changed, whereas the realized gain shows differences depending on the frequency. With respect to the without corrugation case, the realized gain of the antenna increases by placing a corrugation over the frequency range between 2 GHz and 7 GHz.

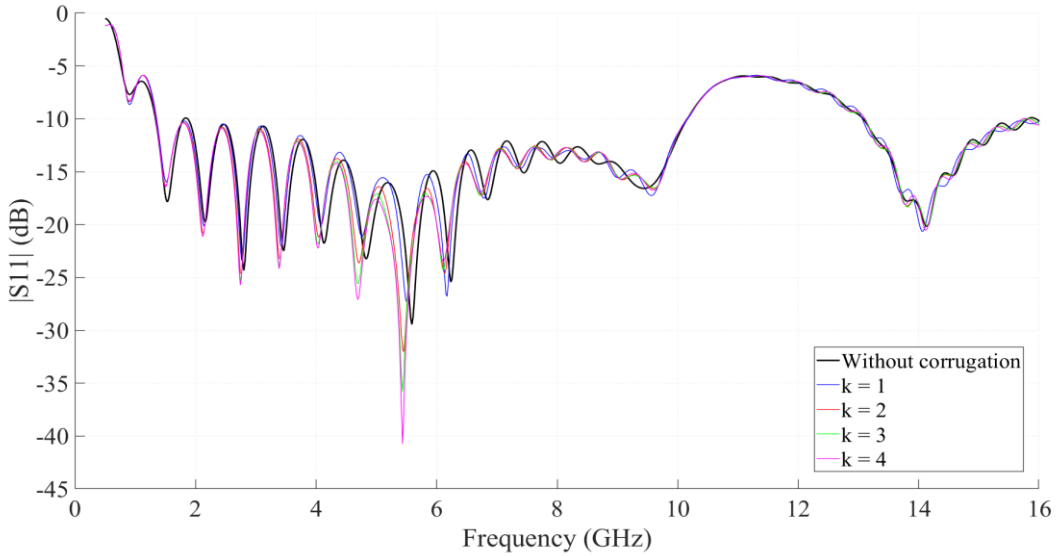

(a)

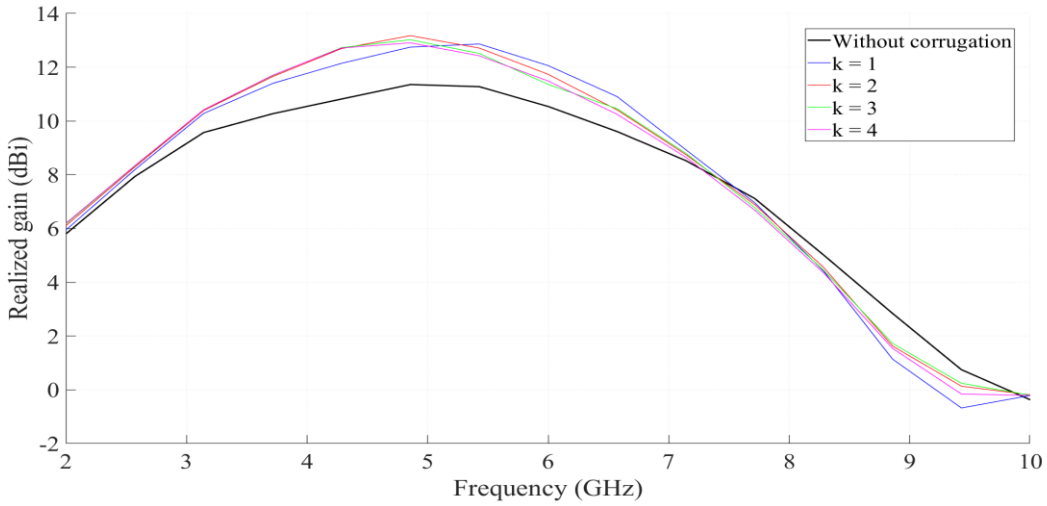

(b)

Figure 3.6 (a) Return loss and (b) realized gain changes of the sine corrugated antenna with constant corrugation amplitude A = 3 mm, and different corrugation periods calculated in the simulations

In retrospect, design guidelines for Vivaldi antennas discussed in Chapter 2 shows that the minimum operating frequency of the antenna depends on the width of its aperture. However, having a wide aperture causes degradations in the far field radiation pattern especially at high frequencies. Therefore, to achieve a directive radiation with high gains at high frequencies, the width of the antenna needs to be scaled down. On the other hand,

as seen in Figure 3.5(a), slight improvements in the return loss of the antenna are achieved as the amplitude of the sine wave corrugation increases. Based on these observations, it can be inferred that if the width of the aperture is reduced and a proper sine wave corrugation is applied, the Vivaldi antenna might still be able to operate in a band with the same lower cutoff frequency, while achieving better radiation characteristics at high frequencies in its operating bandwidth. To verify this inference, a simulation was carried out for different values of the width of the flare, H_f, and the width of the substrate, H_c, without applying a corrugation while the rest of the antenna parameters were kept the same (see Table 3.1). Then, a sine corrugation was applied with the constant period, T = 3.14 mm, $k = 2$ mm^{-1}, and different amplitudes A = 2, 3, 4, and 5 mm. The return loss and the realized gain changes of the antenna with frequency when corrugation is not applied calculated in the simulations are illustrated in Figure 3.7.

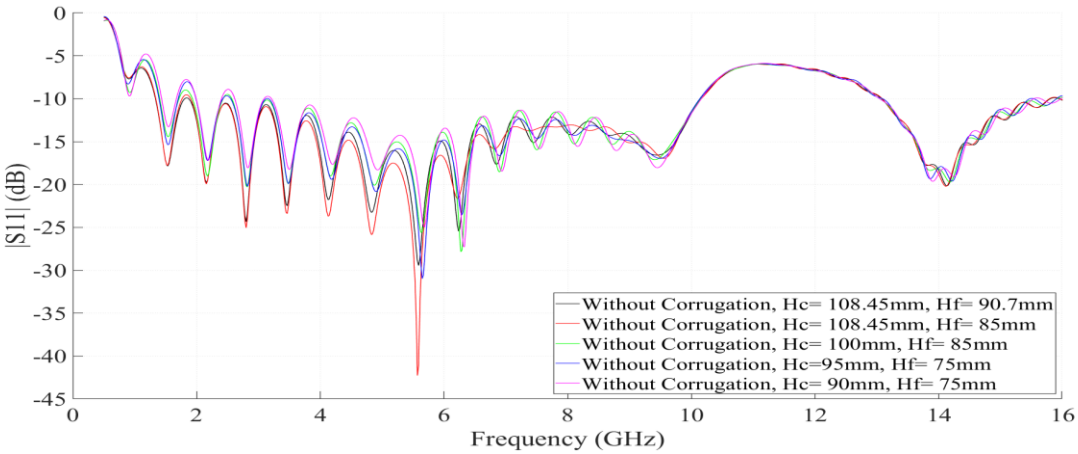

(a)

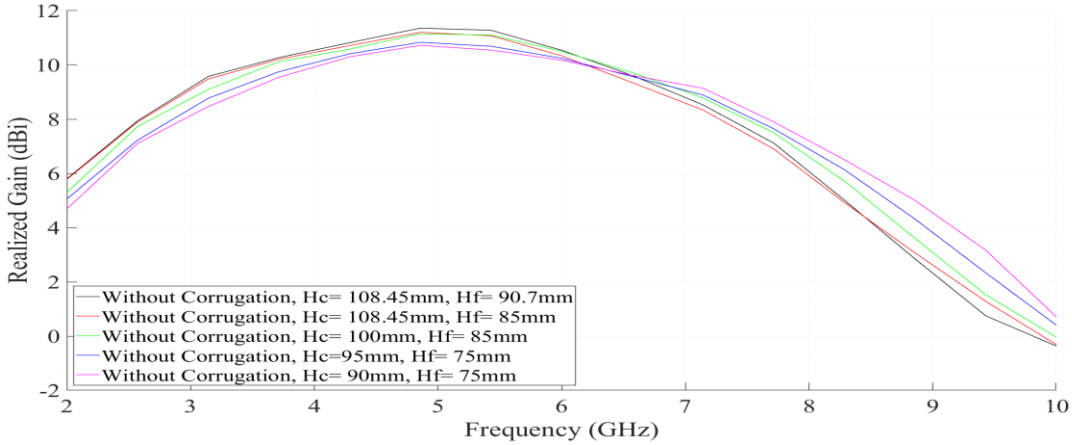

(b)

Figure 3.7 (a) Return loss and, (b) realized gain changes of the antenna without corrugation for different substrate and flare heights

It is seen from the figure that when the width of the substrate and flares shrunk, S11 parameters and the realized gain of the antenna become worse at low frequencies, whereas the realized gain becomes better at high frequencies. However, when a corrugation is applied, with the increasing amplitude of the corrugation, S11 parameters become better especially at low frequencies as seen in Figure 3.8(a). A similar observation is done for the realized gain of the antenna as shown in Figure 3.8(b). However, although the gain at low frequencies is improved, starting from 7 GHz, at high frequencies it gets worse. In other words, despite the decrease of the gain at high frequencies, both the return loss and realized gain of the designed Vivaldi antenna improve at low frequencies by making the aperture to be small and placing a sine corrugation. The applied approach of shrinking the aperture and corrugating the flare sides of the Vivaldi antenna simultaneously is promising in the sense that it can be used as a miniaturization method for Vivaldi antennas.

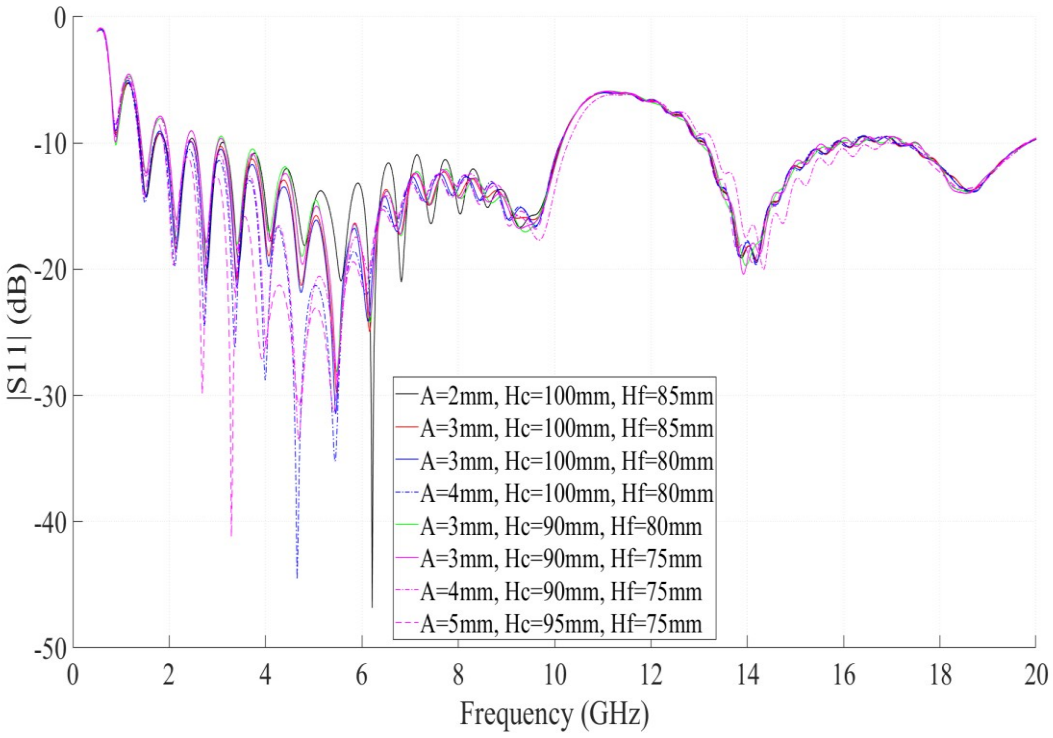

(a)

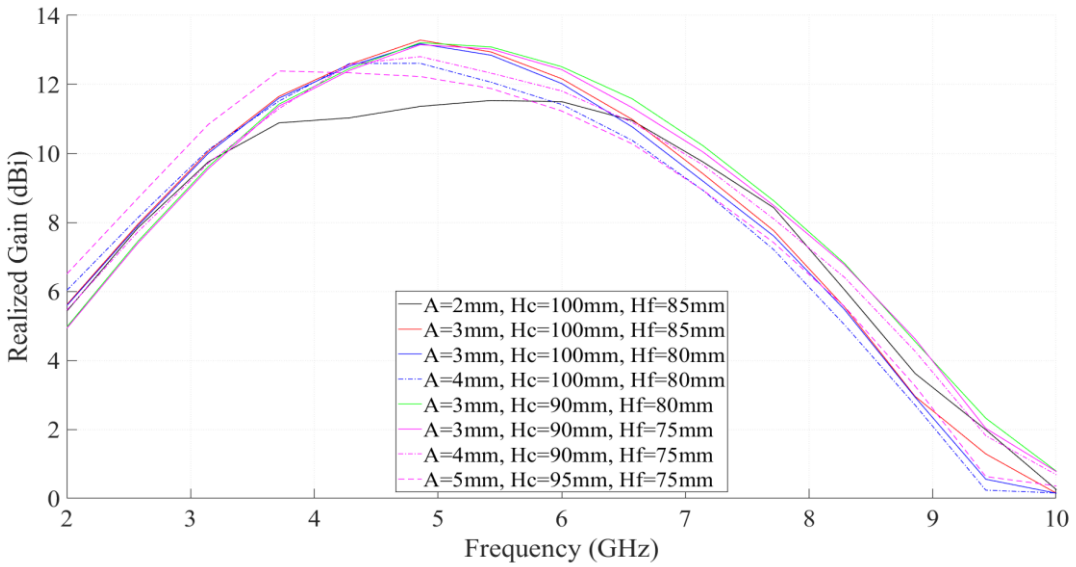

(b)

Figure 3.8 (a) Return loss and (b) realized gain changes of the sine corrugated antenna with the constant corrugation period $k = 2$ and different corrugation amplitudes for different widths of the substrate and exponential flares

For the corrugations applied above, the width of the exponential flares near the aperture of the antenna is a limiting factor on the maximum amplitude of the sine wave that could be used. Due to the structure of the Vivaldi antenna, the total width of the copper plane becomes narrower towards the +x direction as shown in Figure 3.4(a). Although a sine corrugation with a greater amplitude can be applied near the bottom of the antenna, the same amplitude may not be applicable near the aperture. For this reason, a modification was made on the sine corrugation, such that the amplitude of the sine wave was gradually reduced towards the aperture of the antenna with a fixed exponential decay factor. To realize this, Equation 3.1, which defines the profile of the sine corrugation is modified as Equation 3.6 below

$$y = \exp(-f) * A * \sin(kx) \tag{3.6}$$

where f is the constant with which the amplitude of the sine wave reduces towards the aperture of the antenna. The structure of the antenna with a sine corrugation whose profile is defined by Equation 3.6 is shown in Figure 3.9.

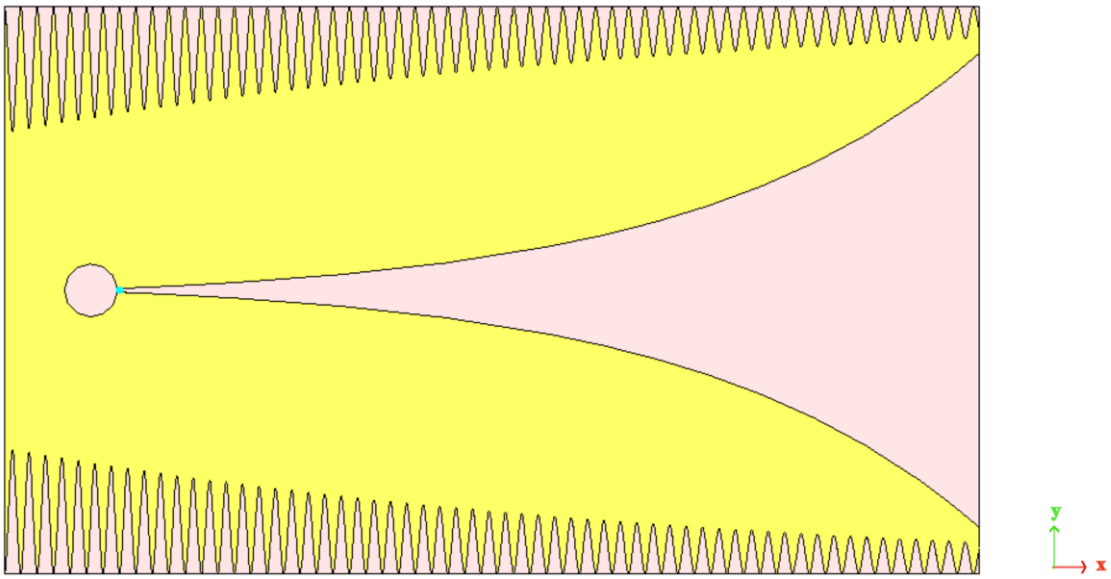

Figure 3.9 Top view of the antenna with a sine corrugation of nonuniform amplitude.

Next, simulations were repeated for the antenna having nonuniform sine corrugation with different amplitudes and decay factors. In the simulations the geometrical parameters of the antenna are set identical to those shown in Table 3.1. Figure 3.10 shows the S11 parameter and realized gain changes of the antenna with the nonuniform sine corrugation, where the constant decay factor f is equal to 0.005 and different amplitudes of the sine wave, i.e., the parameter A equals to 8 mm, 10 mm and 12 mm. It is seen from the figure that applying a sine corrugation with a greater amplitude further improves the impedance matching and realized gain of the antenna at lower frequencies, although it has adverse effects on the realized gain at higher frequencies. Based on this observation, it can be inferred that the parameters of the sine corrugation can be further analyzed to exploit the best performance of the antenna, especially at lower frequencies. To further elaborate on the effects of the sine corrugation having a nonuniform amplitude, simulations were repeated where the amplitude of the sine wave, A, was kept constant at 12 mm and different values of the decay factor, i.e., f equals to 0.005, 0.0075 and 0.01, were used. It is seen from Figure 3.11(a) that using different values of the decay factor, f, does not drastically change the S11 parameters of the antenna. However, Figure 3.11(b) shows that when the decay factor is greater, i.e. the amplitude of the sine wave becomes lower at a faster rate, the realized gain of the antenna becomes worse at lower frequencies, while it becomes better at higher frequencies. Based on the proper selection of the corrugation parameters, S11 parameters and the realized gain of the antenna can be tuned for the desired performance at certain frequencies.

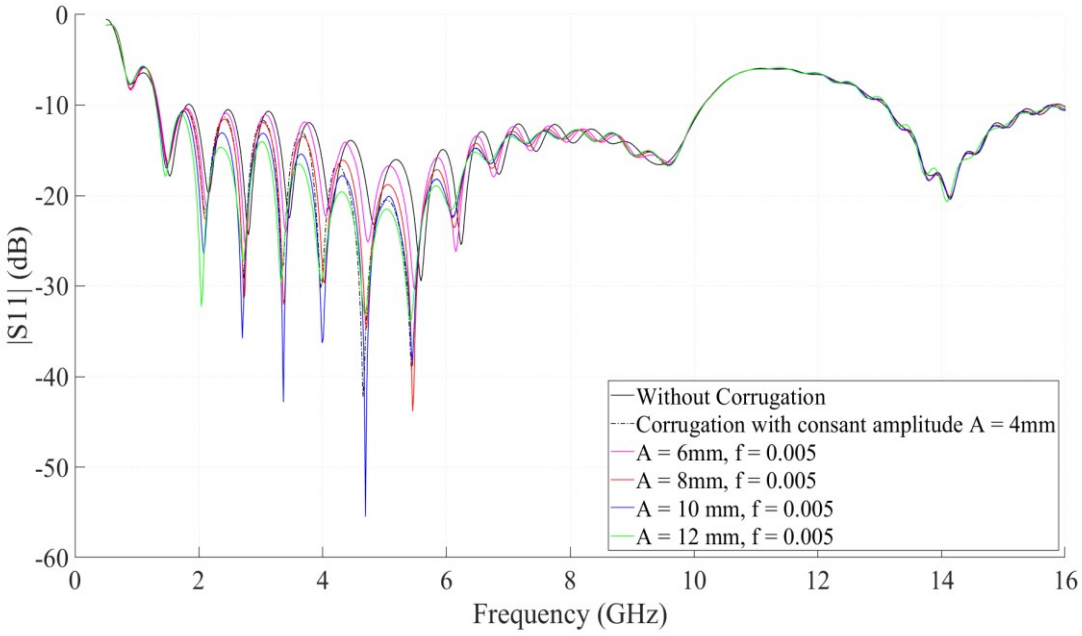

(a)

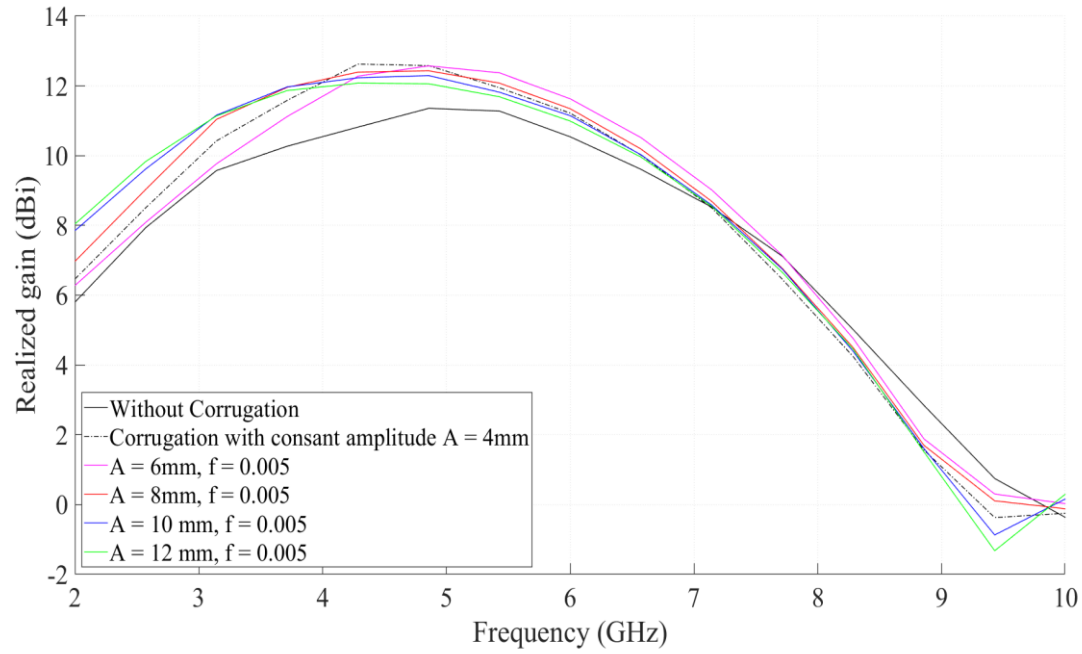

(b)

Figure 3.10 (a) S11 and (b) realized gain changes of the sine corrugated antenna with the sine corrugation having a constant period and nonuniform amplitude

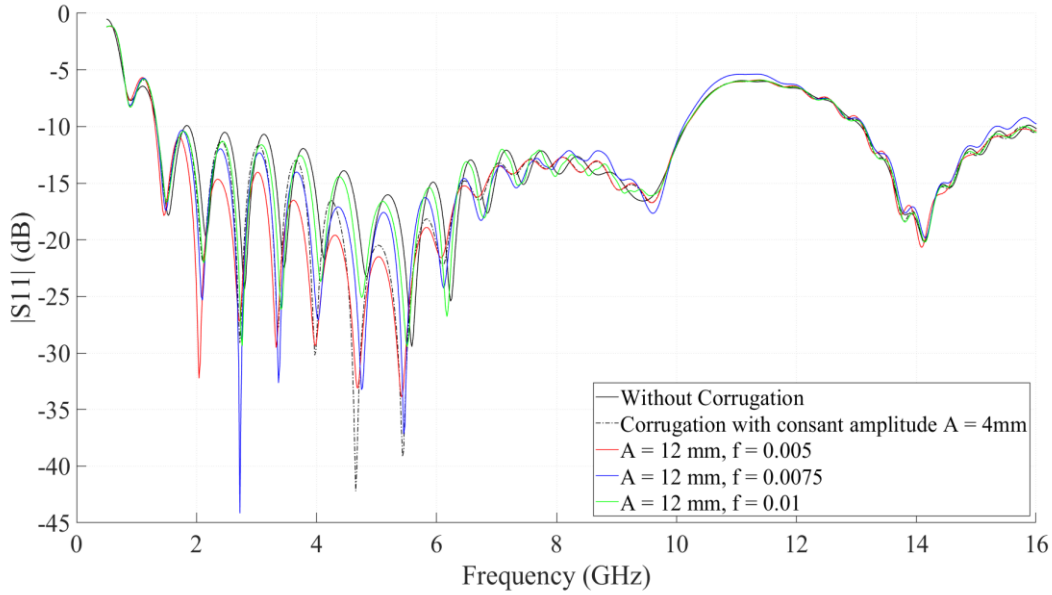

(a)

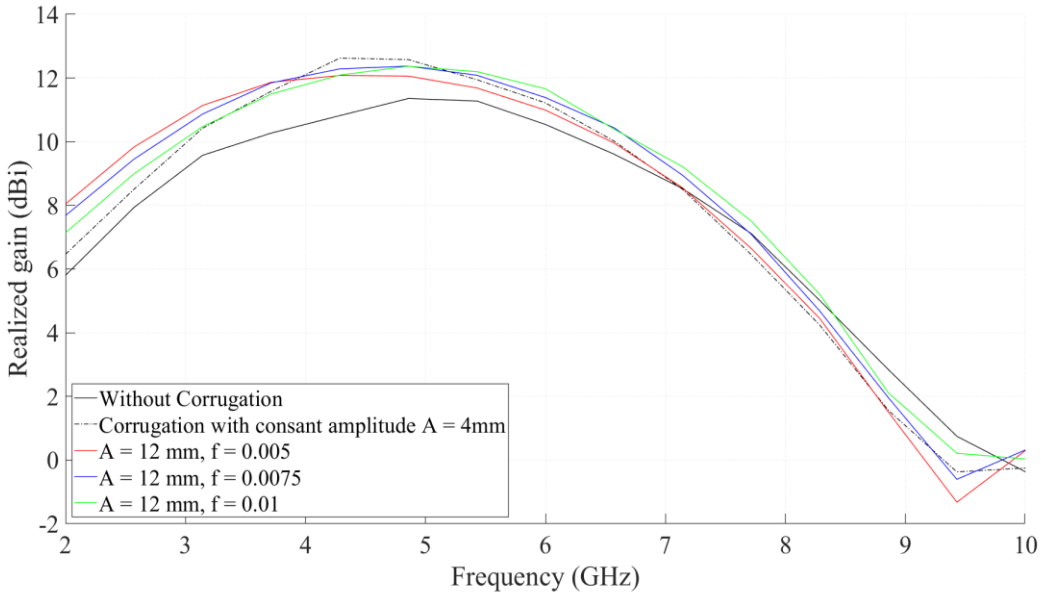

(b)

Figure 3.11 (a) S11 and (b) realized gain changes of the sine corrugated antenna with sine amplitude A = 12 mm and different amplitude decay factors

After analyzing the effects of the sine corrugation with a nonuniform amplitude, a different analysis was performed where the amplitude of the sine corrugation is kept constant and a nonuniform periodicity is applied. To realize this structure, the equation which defines the profile of the sine corrugation is modified to Equation 3.7 below

$$y = A * \sin(f * k * x) \tag{3.7}$$

where f is the constant by which the periodicity of the sine wave is modulated. The structure of the sine corrugated Vivaldi antenna with a constant corrugation amplitude and nonuniform periodicity is shown in Figure 3.12.

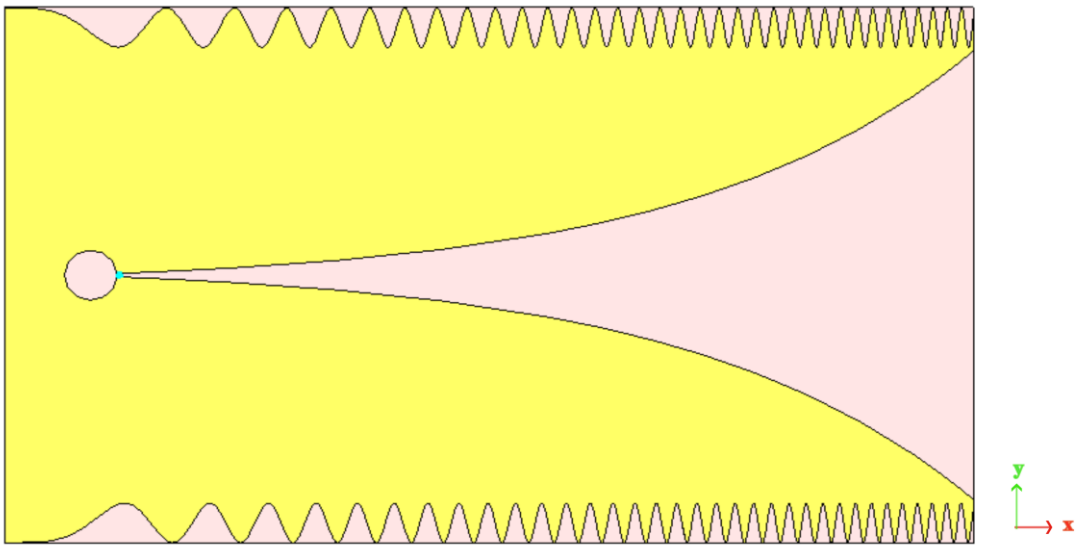

Figure 3.12 Top view of the sine corrugated Vivaldi antenna with a constant corrugation amplitude and nonuniform periodicity

Simulations were repeated for the sine corrugated antenna having the constant corrugation amplitude, A, equal to 4 mm and initial corrugation periodicity, k = 1 mm^{-1} and 2 mm^{-1}, where the periodicity of the sine wave is modulated with different values of the parameter f. It is seen from Figure 3.13 that modulating the periodicity of the sine wave does not have a significant effect on the antenna's S11 parameters and the realized gain.

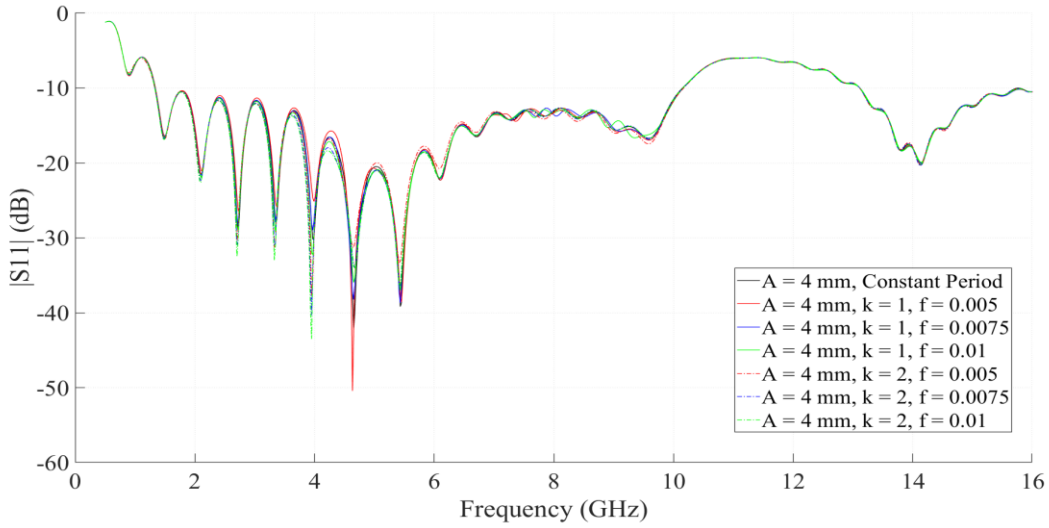

(a)

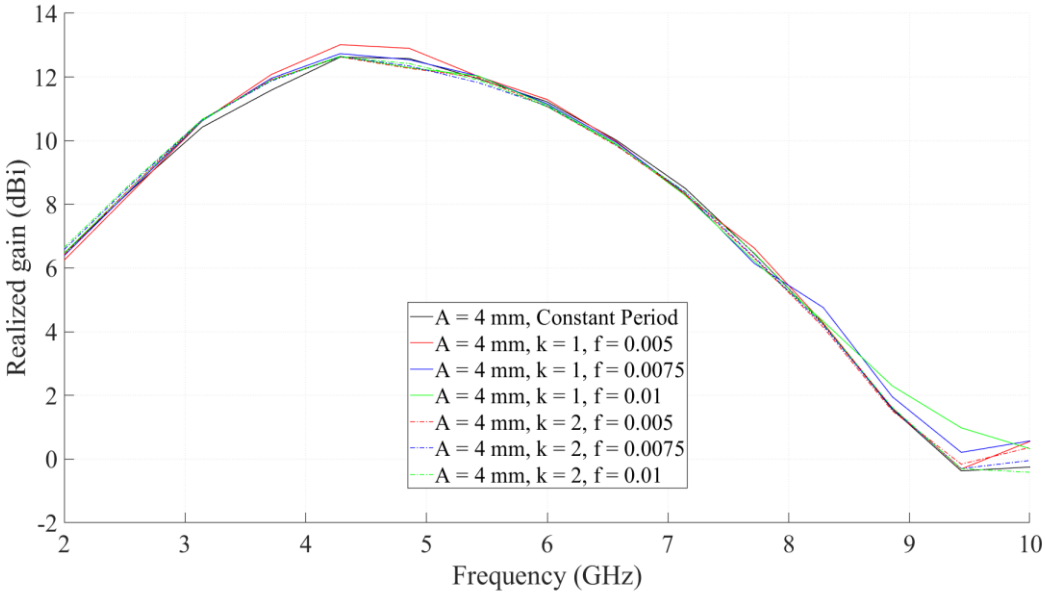

(b)

Figure 3.13 (a) S11 and (b) realized gain changes of the antenna having sine corrugation with constant corrugation amplitude, A = 4 mm, and nonuniform periodicity

3.3 Parasitic patch and dielectric lens

Yet another performance enhancement technique for Vivaldi antennas found in the literature is the use of parasitic patches or dielectric lenses placed at the antenna's aperture. Parasitic patches are often designed and placed between the tapered flares, where they couple with the electric fields generated between the flares and focus the radiated beam and by so doing they improve the gain of the antenna [54]. The shape of the parasitic patch can take many forms. For example, in [55] an elliptical patch is used to improve the performance of an AVA, whereas in [56] a rectangular patch is used. Furthermore, in [57], a diamond shaped parasitic patch is presented. Other forms of parasitic patches or directors found in the literature are in the form of metamaterial-based surfaces. The metamaterial surface consists of an array of unit cells, where the unit cell is defined with different types of materials, for example, epsilon negative, mu negative, isotropic, anisotropic etc. [58-59]. The geometry of the unit cells can take many different forms. However, the design and implementation of such surfaces is challenging. Dielectric lens is often used as a complimentary method to parasitic patch, and they are often designed by extending the substrate from the aperture in a certain geometry. Then, the parasitic director is placed on the lens. For example, in [60], a dielectric lens in the

form of a half circle is placed at the aperture of the AVA, then a circular parasitic patch is placed at the lens. In the following chapter, the effect of placing a diamond shaped parasitic patch at the antenna aperture will be analyzed.

3.3.1 Design and simulation results of the Vivaldi antenna with circular cavity, radial stub terminated microstrip feed and diamond shaped patch

The geometry of the diamond shaped patch presented in this chapter consists of two triangles placed back-to-back, where the height of the first triangle, h_{t1}, pointed towards the linear slot is 12 mm, and the height of the second triangle, h_{t2}, pointed towards the antenna aperture is 30 mm. The width of these triangles, i.e. the height of the diamond h_d, is 10 mm. Other geometrical parameters of the antenna are identical to those provided in Table 3.1. The structure of the antenna with diamond shaped parasitic patch is shown in Figure 3.14.

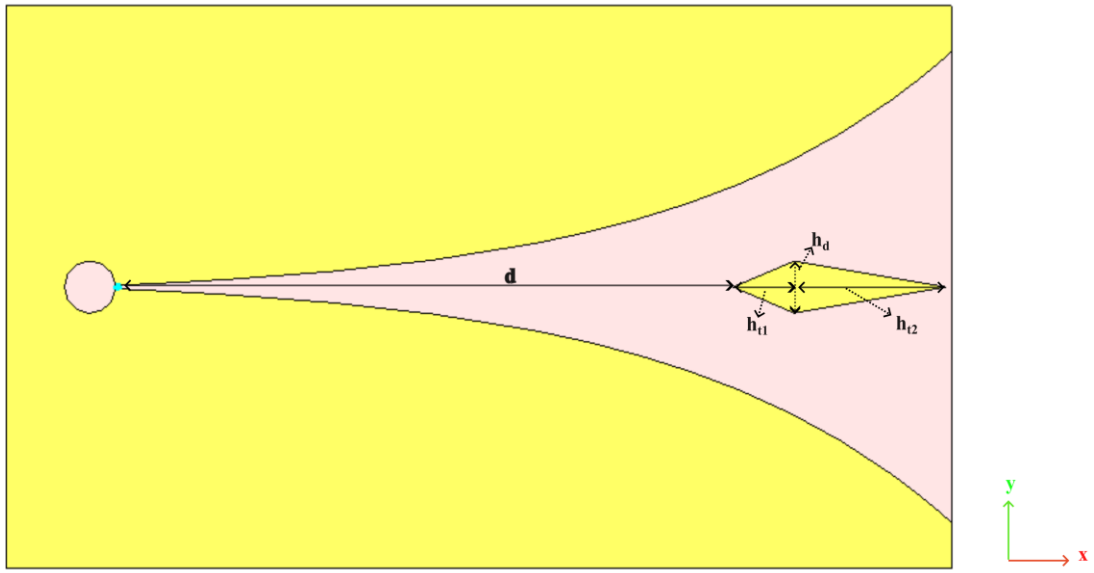

Figure 3.14 Structure of the Vivaldi antenna with diamond shaped parasitic patch

As shown in Figure 3.14 above, the parasitic patch is placed at the center of the antenna with the distance d of the corner closest to the linear slot is 100 mm. A comparison of the return loss and realized gain of the Vivaldi antenna with and without the parasitic patch is shown in Figure 3.15. It is seen that adding a parasitic patch between the exponential flares of the antenna results in an improved gain at higher frequencies while it does not have a significant impact on the return loss. To further analyze the effect of the parasitic patch, a parametric sweep was carried out where the parasitic patch is

moved towards the antenna aperture until distance d of the corner closest to the linear slot reached 121 mm with 3 mm steps. The changes in the return loss and realized gain of the antenna depending on the position of the parasitic patch are shown in Figure 3.16.

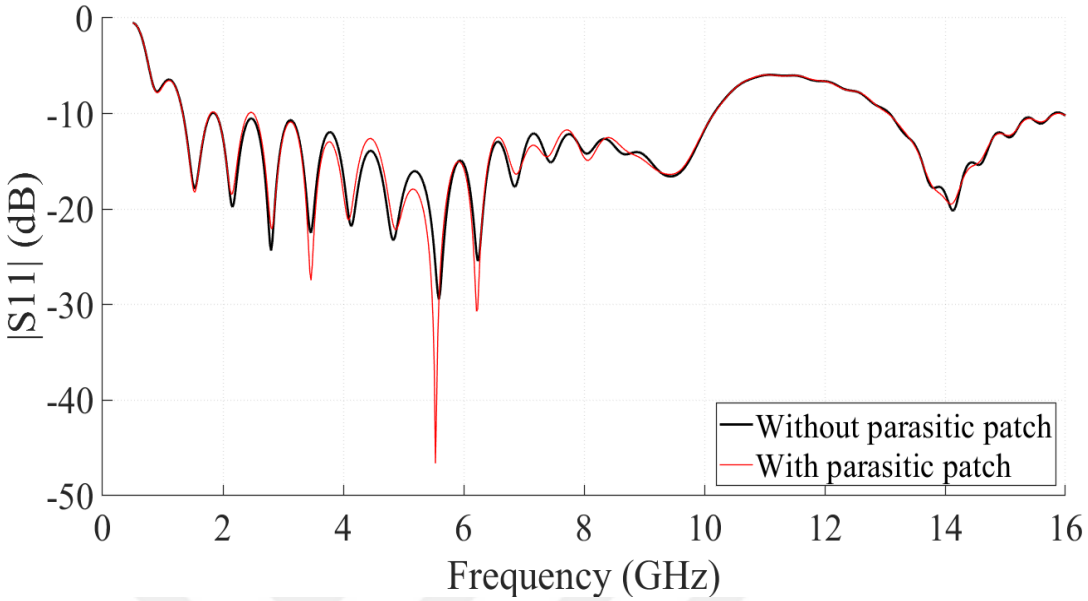

(a)

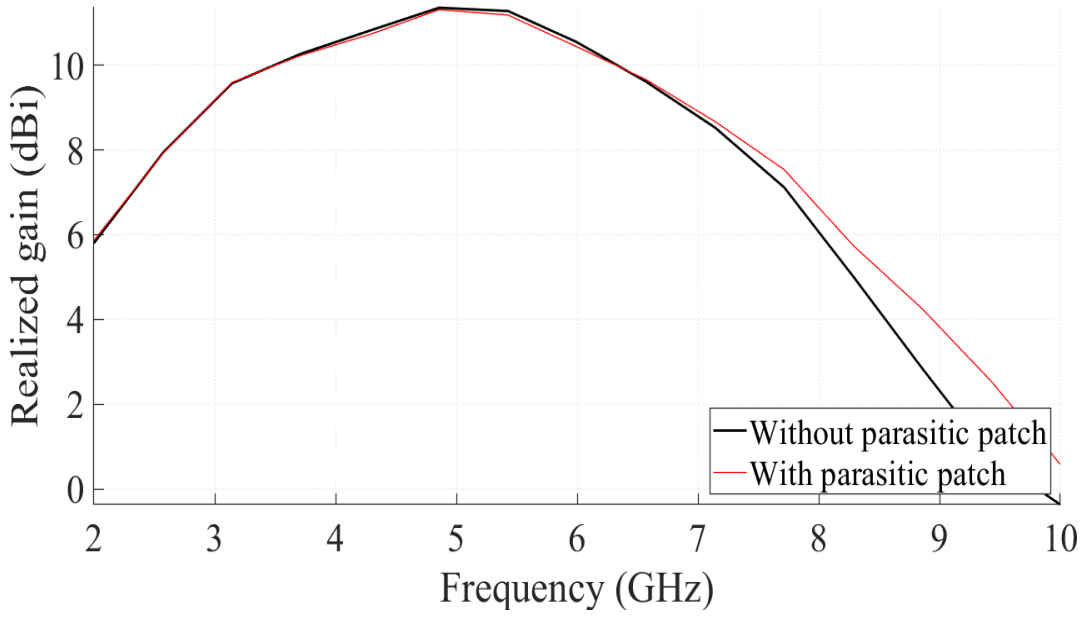

(b)

Figure 3.15 (a) Return loss and (b) realized gain of the antenna with and without parasitic patch

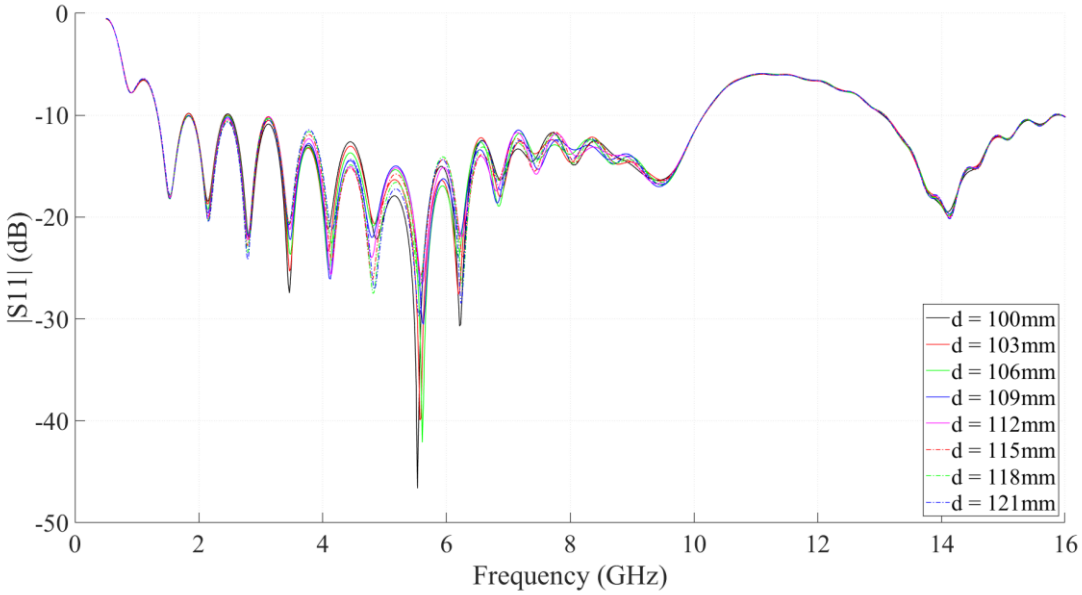

(a)

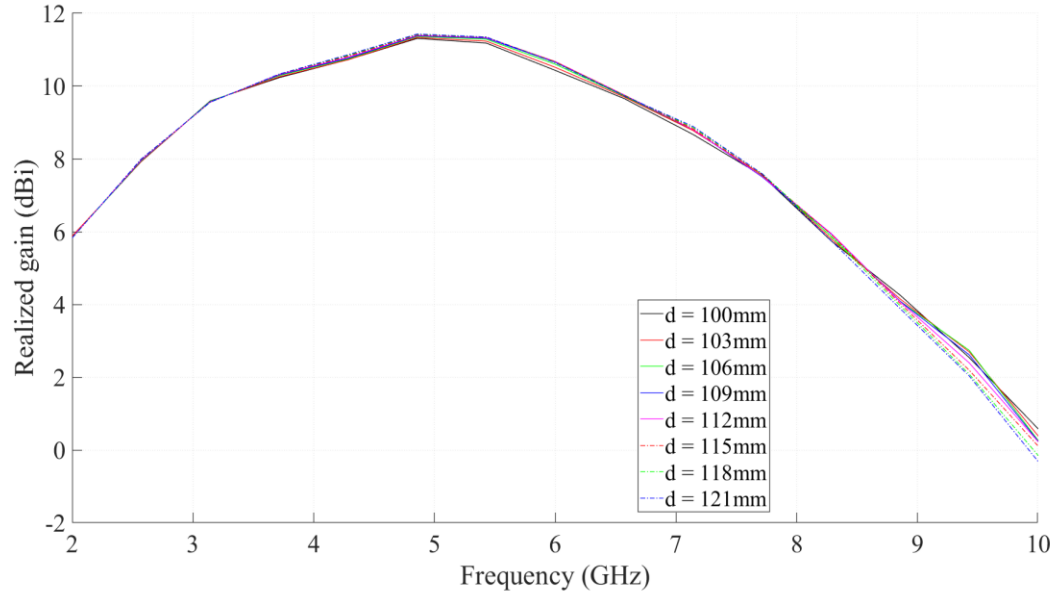

(b)

Figure 3.16 (a) Return loss and (b) realized gain changes of the antenna for different positions of the diamond shaped parasitic patch

From the figure, it is seen that a similar behavior in the return loss and the realized gain is observed as the parasitic patch is moved further up towards the aperture. It is important to note that as the parasitic patch is moved towards the aperture, the distance between the flares and the patch increases, which impacts the coupling between them. For this reason, simulations were repeated while the position of the diamond patch was kept constant at d = 121 mm, while the width of the triangles that form the diamond structure,

i.e. the width of the diamond patch along the y axis, was increased from 10 mm to 20 mm in 2 mm steps. The results of these simulations are shown in Figure 3.17. It is seen from the figure that, when the position of the parasitic patch is constant, increasing its width causes the deep and peak points of the S11 trace to become lower and higher, respectively. Furthermore, the frequencies at which the deep and peak points appear do not change significantly. Based on the observations from Figures 3.16 and 3.17, it is understood that with the proper selection of the position and size of the diamond shaped parasitic patch, it may be possible to improve the gain of the Vivaldi antenna at select frequencies, although it may be at the cost of worsening the achieved gain at other frequencies.

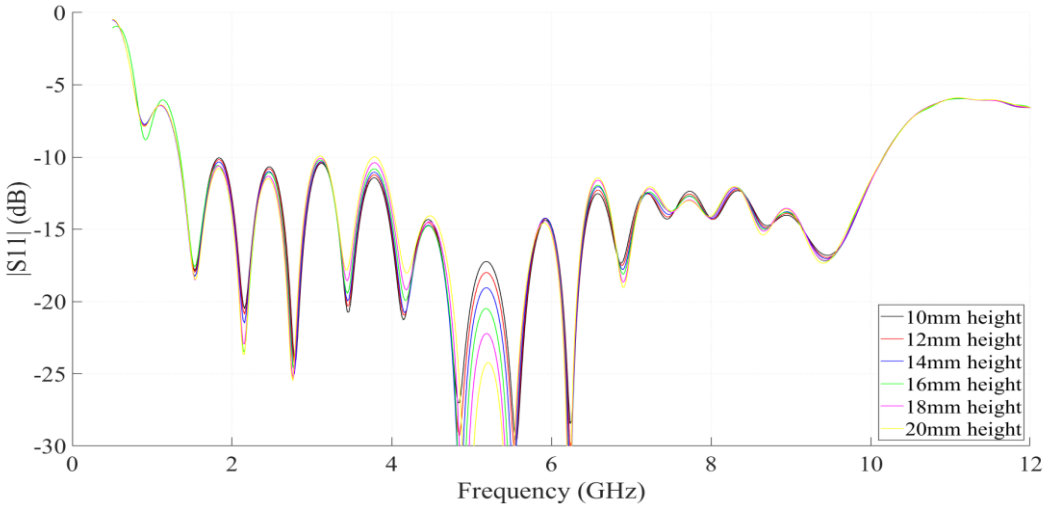

(a)

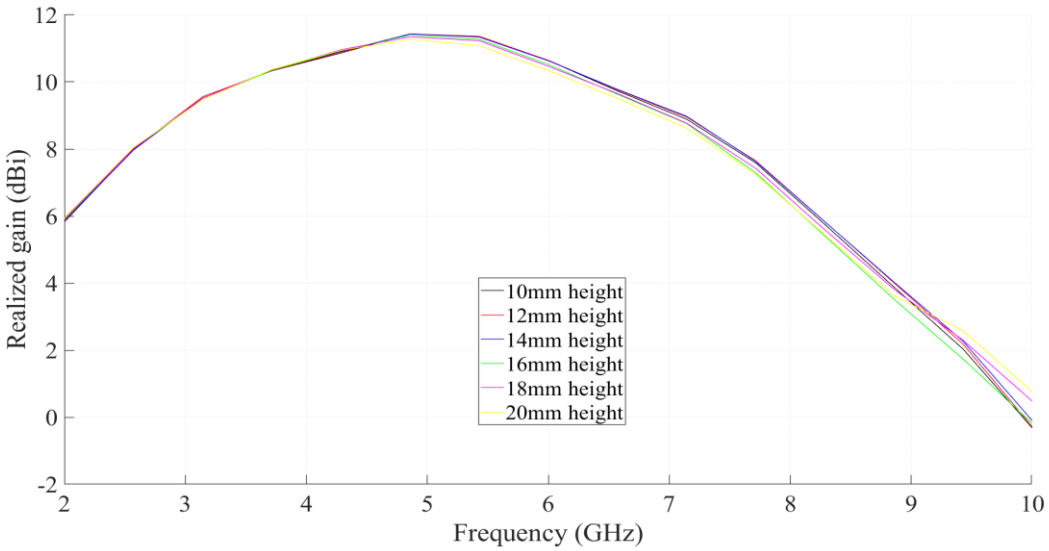

(b)

Figure 3.17 (a) Return loss and (b) realized gain changes of the antenna for different widths of the parasitic patch

After this analysis, the parasitic patch structure was implemented with the sine corrugation presented in the previous chapter. The structure of the Vivaldi antenna with the sine corrugation and the parasitic patch is shown in Figure 3.18. Simulations were repeated for the antenna having a sine corrugation with the corrugation amplitude, A = 4 mm, and period T = 3.14 mm, k = 2 mm^{-1}, and a parasitic patch placed in the antenna aperture which is identical to the one presented in Figure 3.14. The S11 parameter and realized gain changes of the antenna with the sine corrugation and parasitic patch for the different positions of the parasitic patch are shown in Figure 3.19 and Figure 3.20. From the figures, it is seen that the negative effects of placing a parasitic patch in the antenna aperture on S11 parameters at low frequencies are mitigated by applying the sine corrugation. This is also seen in the realized gain of the antenna as can be seen from Figures 3.19(b) and 3.20(b). However, at higher frequencies, using the parasitic patch without a sine corrugation yields better results in the realized gain of the antenna. Therefore, depending on the desired performance, a tradeoff can be made between using a parasitic patch with or without a sine corrugation.

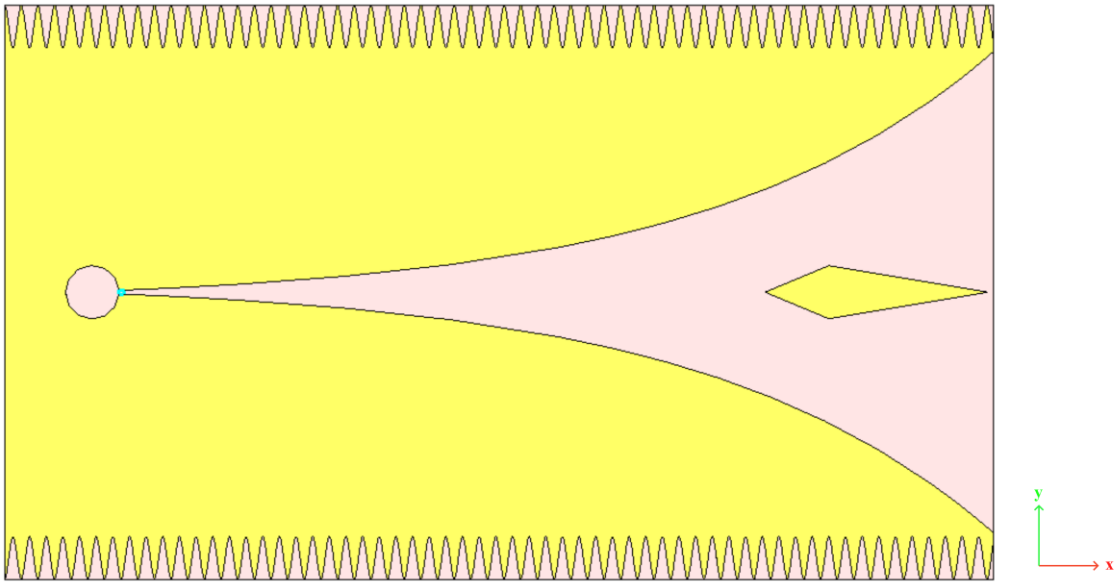

Figure 3.18 Structure of the Vivaldi antenna with a sine corrugation and diamond shaped parasitic patch

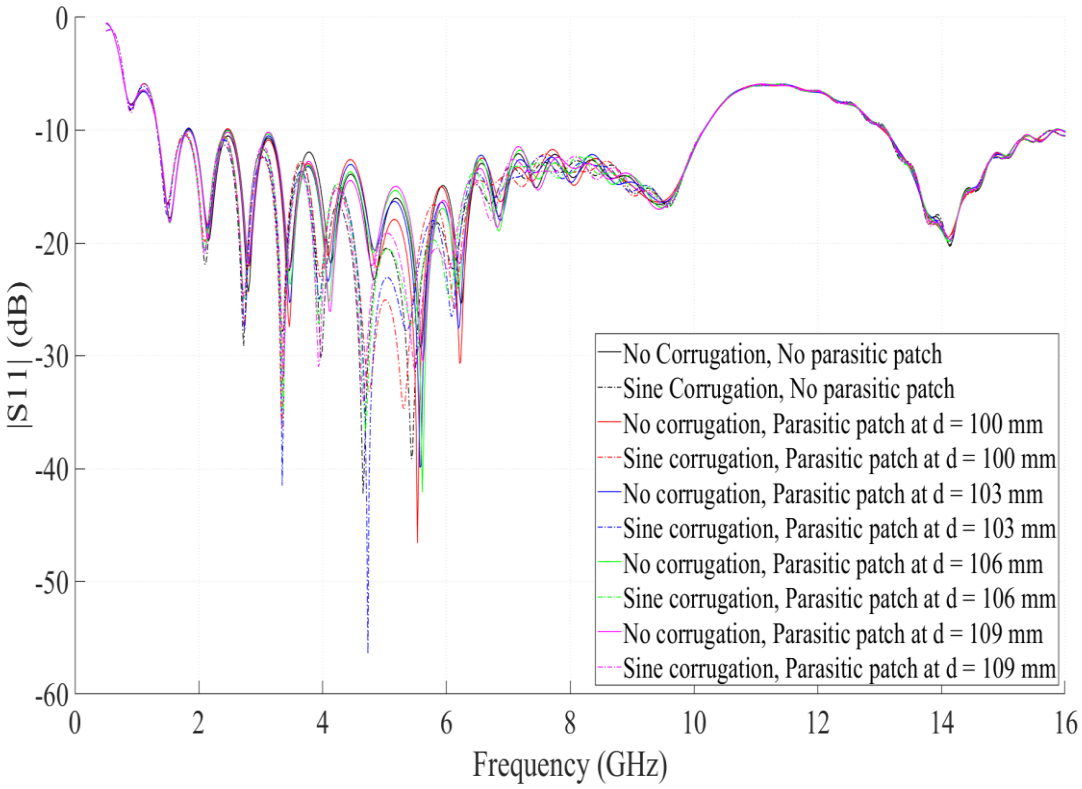

(a)

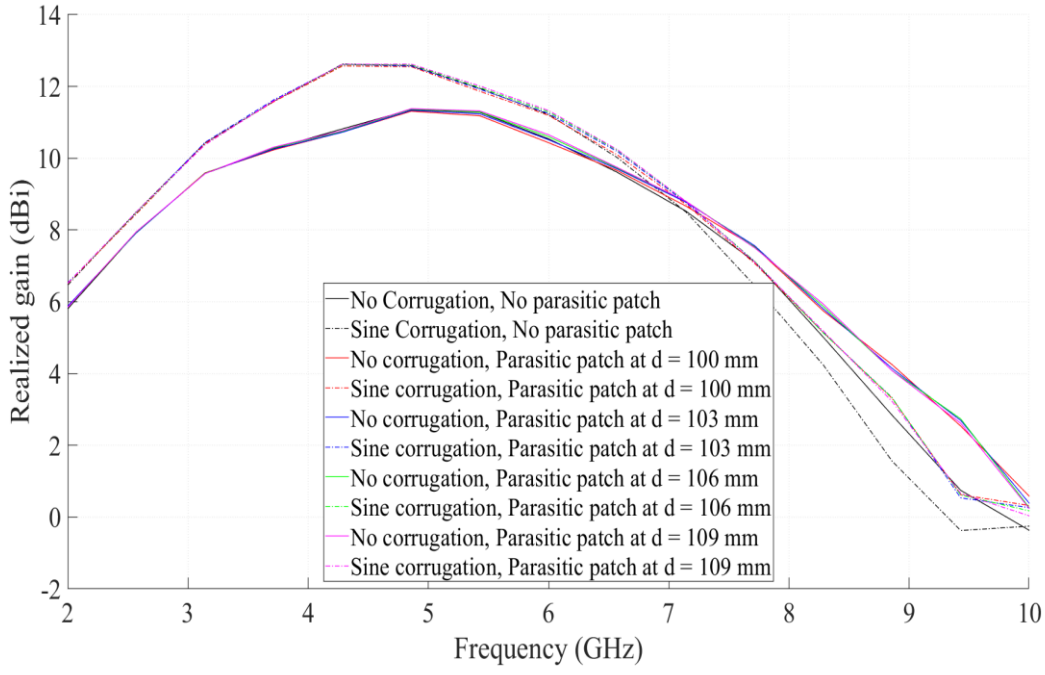

(b)

Figure 3.19 (a) S11 parameter and (b) realized gain changes of the antenna with the parasitic patch and sine corrugation calculated in the simulations for different positions of the parasitic patch between d = 100 mm and d = 109 mm

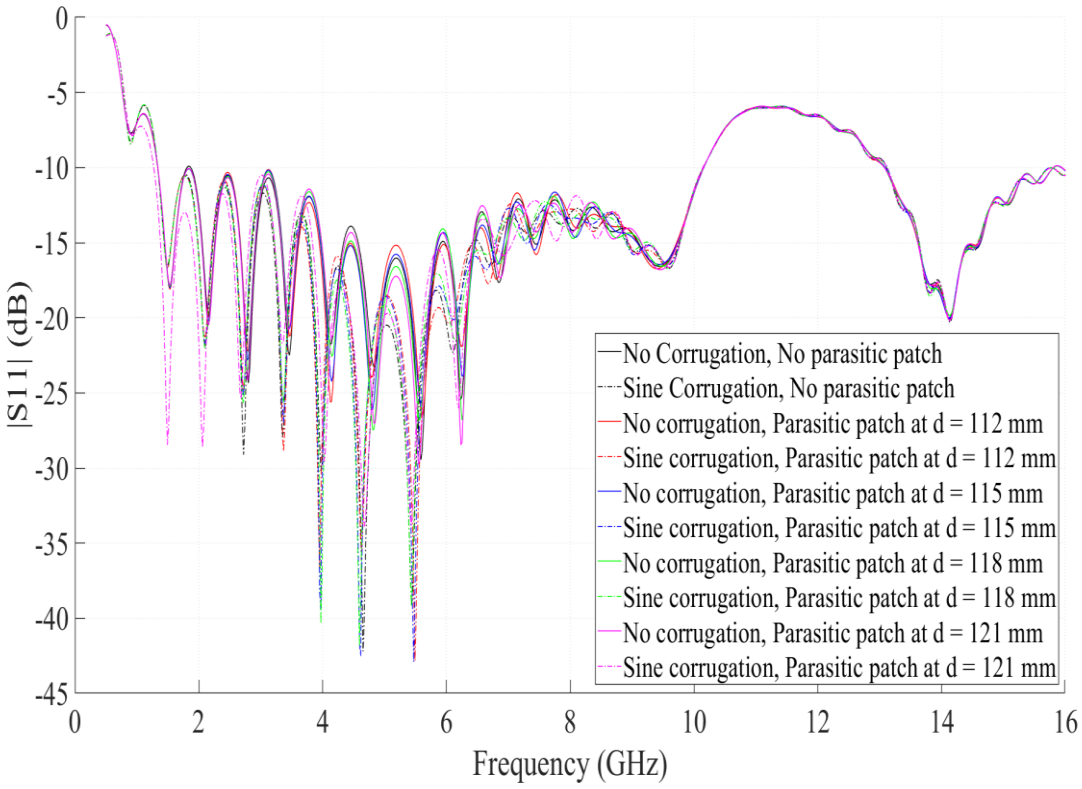

(a)

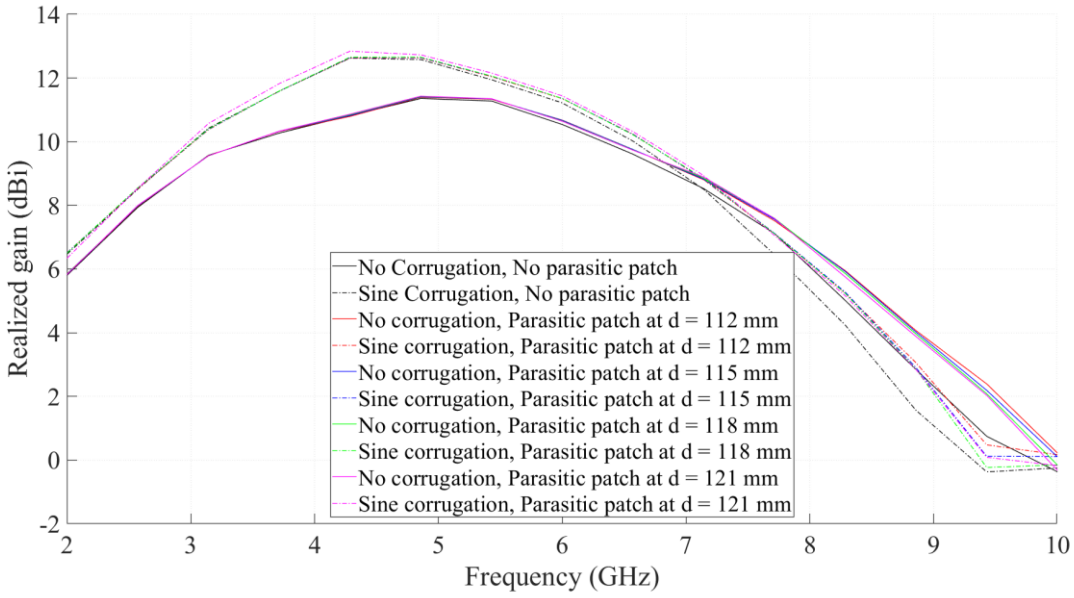

(b)

Figure 3.20 (a) S11 parameter and (b) realized gain changes of the antenna with the parasitic patch and sine corrugation calculated in the simulations for different positions of the parasitic patch between d = 112 mm and d = 121 mm

Chapter 4

Conclusions and Future Prospects

4.1 Conclusions

In this research, design of Vivaldi antennas for ultra-wideband communication systems and several performance enhancement techniques were studied. First, using the theoretical guidelines, a Vivaldi antenna with a rectangular microstrip feed which can operate in the ultra-wideband frequencies 3.6 to 10.1 GHz was designed. Using a commercially available three-dimensional electromagnetic simulation tool, the designed antenna was simulated, and its geometrical parameters were optimized. This optimized antenna had a -10 dB impedance bandwidth between 3.1 and 13.6 GHz, and an average realized gain of 2.75 dBi over its bandwidth. Next, a parametric study on the microstrip feed network of the antenna was conducted. There were two parameters of the microstrip feed that was investigated. The first parameter, namely QWs, is the longitudinal displacement of the feed along the linear slot on conducting plane. The second parameter, namely QWm, is the length of the microstrip that exceeds the linear slot. The analysis on these two parameters showed that one can adjust the lower and higher cutoff frequencies of the antenna, thus tune the bandwidth of the antenna while mostly preserving the radiation characteristics, by changing only the location and total length of the microstrip feed. This may assist the antenna designer in the sense that the parameters for antenna can be approximated for a desired bandwidth and without the need for extensively analyzing other geometrical parameters, the design can be made to fit the desired bandwidth by analyzing the parameters related to the microstrip feed.

Some of the main limitations of the antenna mentioned above are its poor radiation characteristics at the lower and higher ends of the bandwidth, and low gain. This is mainly due to the impedance mismatch between the 50 Ω microstrip feed and the high impedance metal surface at the linear slot. Furthermore, it is sometimes more desirable to design the

UWB antenna not only to cover the 3.6-10.1 GHz UWB frequencies, but also to cover the frequencies at the unlicensed Industrial, Scientific and Medical (ISM) band for applications such as 2.4 GHz WiFi. Achieving this with the initial design of the Vivaldi antenna is not very feasible as the geometrical size required for such an antenna would be very large. Therefore, to overcome these limitations, some of the performance enhancement techniques found in the literature was studied and applied on the designed antenna.

The first enhancement technique covered in this research was changing the 50 Ω microstrip feed to a balun structure, terminated with a radial stub. The balun is designed to have 50 Ω impedance at the input port and 100 Ω impedance at the linear slot. This 50 Ω to 100 Ω transition was with the purpose of providing better impedance matching at the microstrip-to-slot line transition. On the other hand, terminating the balun with a radial stub serves the purpose of minimizing the reflections that occur on the feed line. To further reduce the reflection at the microstrip-to-slot line transition, a circular cavity was also added before the linear slot. The antenna designed with this technique demonstrated -10 dB impedance bandwidth between the frequencies 1.33 GHz and 10.1 GHz, and an average realized gain of 6 dBi over the bandwidth.

The next enhancement technique studied in this research was corrugation applied to the sides of the flares of Vivaldi antenna. Although there are several types of corrugation found in the literature, sine wave corrugation was adopted in this study. The main purpose of using corrugation is to minimize the surface currents that occur on the sides of the flares, and by so doing, reducing the sidelobe levels and achieving better directivity, and improving the return loss, i.e. S11 parameters, of the antenna. With the implementation of sine wave corrugation, realized gains as high as 13.1 dBi was achieved near the center frequency of the antenna. From the analysis on the sine wave corrugation, it was found that this method could also be used as a miniaturization technique for Vivaldi antennas. After this analysis, sine corrugation having a nonuniform amplitude and periodicity was also investigated. Although other corrugation structures for coplanar Vivaldi antennas such as rectangular corrugation with nonuniform amplitude have been reported in the literature, to the best of our knowledge, sine corrugation with a nonuniform amplitude and periodicity have not been reported before. The main motivation for applying such corrugation is that due to the exponentially tapered profile of the flares, the radiating plane becomes narrower near the antenna’s aperture. This means that the

maximum corrugation amplitude that can be applied is limited by the width of the exponential flare near the aperture. However, since the radiating plane is not narrow near the input port of the antenna, corrugation with greater amplitude can be applied at the lower region of the antenna. Simulation results showed that by selecting a greater corrugation amplitude near the input port and modulating the amplitude to become smaller near the aperture allows for achieving better impedance matching and higher realized gain at lower frequencies, whereas modulating the periodicity of the sine corrugation does not have a significant effect on the antenna performance.

The last enhancement technique applied to the Vivaldi antenna was adding a parasitic patch (director) between the exponentially tapered flares. It was found that with the proper selection of the position and dimension of the parasitic patch, realized gain of the antenna can be improved at certain frequencies, although the electromagnetic coupling between the patch and the flares could cause degradation of the realized gain and return loss at other frequencies. When the parasitic patch was applied together with the sine corrugation, however, it was seen that at lower frequencies, the sine corrugation is mitigating the negative effects of placing a parasitic patch on the S11 parameter of the antenna and it results in a better realized gain. At higher frequencies, however, applying parasitic patch without the sine corrugation results in a higher realized gain.

4.2 Societal Impact and Contribution to Global Sustainability

UWB technology offers promising solutions for applications such as high precision ranging, asset tracking and high-speed data transfer even in congested networks. Due to these features, UWB systems can be implemented in industrial sites where there are often a great number of devices, e.g. ground or air robots, sensors and asset tags, need to be interconnected in an indoor positioning system [61]. UWB radar systems can be implemented in crowded areas, e.g. airports, malls and train stations, to keep track of the number of people within an area with high accuracy. This, together with the high precision ranging and high-speed data transfer capabilities of UWB systems can be extremely

useful for emergency situations, such as search and rescue during an earthquake [62-64]. Aside from these features, UWB systems are designed to operate on low power levels.

The implementation of UWB communication systems for emergency situations might prove more effective compared to other technologies, and it could save the lives of people. In this sense, the development of UWB systems would have a very positive impact on the society. Furthermore, industrial applications based on ultra-wideband technology might prove more energy efficient compared to other communication standard. Considering this, it may be said that the development of UWB technology would not only have a positive impact on the society, but also contribute towards global sustainability by promoting low energy consumption.

4.3 Future Prospects

In this research, the suitability of Vivaldi antennas for UWB communications was shown. However, for a successful implementation of these antennas in UWB systems, there are more aspects that needs to be considered, such as coverage area of the antenna. While the directive radiation patterns of the Vivaldi antenna may be favorable for certain applications, if a wider area of coverage is required it may be necessary to design an array of multiple antennas, which was not studied in this research.

Another limitation of this study is that it is based solely on computer design and simulation. Although commercial electromagnetic simulation tools are often accurate in their estimations, it may still be necessary to build a prototype of the presented antennas and verify their performance with real measurements.

BIBLIOGRAPHY

[1] T. W. Barrett, “History of Ultra Wideband Communications and Radar: Part I, UWB Communications,” Microw J (Int Ed), vol. 44, no. 1, 2001.

[2] R. Aiello and A. Batra, Ultra Wideband Systems: Technologies and Applications. 2006. doi: 10.1016/B978-0-7506-7893-3.X5000-7.

[3] Liuqing Yang and G. B. Giannakis, “Ultra-wideband communications - An idea whose time has come,” IEEE Signal Process Mag, vol. 21, no. 6, 2004, doi: 10.1109/msp.2004.1359140.

[4] J. Ma et al., “Push the Limit of Highly Accurate Ranging on Commercial UWB Devices,” Proc ACM Interact Mob Wearable Ubiquitous Technol, vol. 8, no. 2, p. 27, May 2024, doi: 10.1145/3659602.

[5] M. R. Mahfouz, A. E. Fathy, M. J. Kuhn, and Y. Wang, “Recent trends and advances in UWB positioning,” in IEEE MTT-S International Microwave Workshop Series on Wireless Sensing, Local Positioning and RFID, Proceedings, IMWS 2009 - Croatia, 2009. doi: 10.1109/IMWS2.2009.5307895.

[6] F. Zhu, S. Gao, A. T. S. Ho, T. W. C. Brown, J. Z. Li, and J. D. Xu, “Low-profiledirectionalultra-wideband antenna for see-through-wall imaging applications,” Progress in Electromagnetics Research, vol. 121, 2011, doi: 10.2528/PIER11080907.

[7] A. Elsharkawy, K. Naheem, D. Koo, and M. S. Kim, “A uwb-driven self-actuated projector platform for interactive augmented reality applications,” Applied Sciences (Switzerland), vol. 11, no. 6, 2021, doi: 10.3390/app11062871.

[8] Y. Rahayu, T. A. Rahman, R. Ngah, and P. S. Hall, “Ultra wideband technology and its applications,” in 5th IEEE and IFIP International Conference on Wireless and Optical Communications Networks, WOCN 2008, 2008. doi: 10.1109/WOCN.2008.4542537.

[9] Qorvo, “APS003 APPLICATION NOTE REAL TIME LOCATION SYSTEMS An Introduction.”

[10] NXP Semiconductors, “NXP Secure UWB deployed in Samsung Galaxy Note20 Ultra Bringing the First UWB-Enabled Android Device to Market | NXP Semiconductors.” Accessed: Sep. 12, 2024. [Online]. Available: https://www.nxp.com/company/about-nxp/newsroom/NW-SECURE-UWB-SAMSUNG-GALAXY

[11] B. Wang, H. Song, W. Rhee, and Z. Wang, “Overview of ultra-wideband transceivers - System architectures and applications,” Tsinghua Sci Technol, vol. 27, no. 3, 2022, doi: 10.26599/TST.2021.9010044.

[12] A. Rangnekar and K. M. Sivalingam, “Multiple channel scheduling in UWB based IEEE 802.15.3 networks,” in Proceedings - First International Conference on Broadband Networks, BroadNets 2004, 2004. doi: 10.1109/BROADNETS.2004.49.

[13] J. Yang, A. Seyedi, D. Birru, and D. Wang, “Design and performance of Multi-Band OFDM UWB system with multiple antennas,” in IEEE International Symposium on Personal, Indoor and Mobile Radio Communications, PIMRC, 2007. doi: 10.1109/PIMRC.2007.4394705.

[14] M.-G. Di Benedetto, T. Kaiser, A. Molisch, I. Oppermann, C. Politano, and D. Porcino, “UWB Communication Systems—A Comprehensive Overview,” UWB Communication Systems—A Comprehensive Overview, 2006, doi: 10.1155/9789775945105.

[15] D. Ghosh, A. De, M. C. Taylor, T. K. Sarkar, M. C. Wicks, and E. L. Mokole, “Transmission and reception by ultra-wideband (UWB) antennas,” IEEE Antennas Propag Mag, vol. 48, no. 5, 2006, doi: 10.1109/MAP.2006.277157.

[16] A. A. Alsoussa, G. Mansour, and E. Nugoolcharoenlap, “Multiband Printed Monopole Antennas for Mobile Devices,” in Proceeding - 2023 IEEE 3rd International Maghreb Meeting of the Conference on Sciences and Techniques of Automatic Control and Computer Engineering, MI-STA 2023, 2023. doi: 10.1109/MI-STA57575.2023.10169284.

[17] H. A. Mohamed, H. Elsadek, and E. A. Abdallah, “Quad ridged UWB TEM horn antenna for GPR applications,” in IEEE National Radar Conference - Proceedings, 2014. doi: 10.1109/RADAR.2014.6875559.

[18] C. Ozdemir, B. Yilmaz, S. I. Keceli, H. Lezki, and O. Sutcuoglu, “Ultra Wide Band horn antenna design for Ground Penetrating Radar: A feeder practice,” in Proceedings International Radar Symposium, 2014. doi: 10.1109/IRS.2014.6869298.

[19] H. Y. Yu, J. Yu, X. Liu, Y. Yao, and X. Chen, “A Wideband Circularly Polarized Horn Antenna with a Tapered Elliptical Waveguide Polarizer,” IEEE Trans Antennas Propag, vol. 67, no. 6, 2019, doi: 10.1109/TAP.2019.2905789.

[20] M. Puri, P. K. Mishra, S. S. Dhanik, and H. Khubchandani, “Design and simulation of double ridged horn antenna operating for UWB applications,” in 2013 Annual IEEE India Conference, INDICON 2013, 2013. doi: 10.1109/INDCON.2013.6725860.

[21] T. Saeidi, I. Ismail, W. P. Wen, A. R. H. Alhawari, and A. Mohammadi, “Ultra-wideband antennas for wireless communication applications,” 2019. doi: 10.1155/2019/7918765.

[22] O. P. Kumar, P. Kumar, T. Ali, P. Kumar, and S. Vincent, “Ultrawideband Antennas: Growth and Evolution,” 2022. doi: 10.3390/mi13010060.

[23] M. A. Peyrot-Solis, G. M. Galvan-Tejada, and H. Jardon-Aguilar, “State of the art in ultra-wideband antennas,” in 2nd International Conference on Electrical and Electronics Engineering, ICEEE and XI Conference on Electrical Engineering, CIE 2005, 2005. doi: 10.1109/ICEEE.2005.1529583.

[24] M. Y. Abou Shahine, M. Al-Husseini, K. Y. Kabalan, and A. El-Hajj, “Dielectric resonator antennas with band rejection and frequency reconfigurability,” Progress In Electromagnetics Research C, vol. 46, 2014, doi: 10.2528/PIERC13112101.

[25] D. Negi, R. Khanna, and J. Kaur, “Design and performance analysis of a conformal CPW fed wideband antenna with Mu-Negative metamaterial for wearable applications,” Int J Microw Wirel Technol, vol. 11, no. 8, 2019, doi: 10.1017/S1759078719000497.

[26] B. R. Behera, “Vivaldi antenna for UWB communications: Design, modelling and analysis of Vivaldi Antenna with genetic algorithm,” in ICCCCM 2016 - 2nd IEEE International Conference on Control Computing Communication and Materials, 2017. doi: 10.1109/ICCCCM.2016.7918252.

[27] T. O. Praktika, A. A. Pramudita, and Y. Wahyu, “Design of Vivaldi antenna for UWB respiration radar,” in 2019 International Conference on Information and Communications Technology, ICOIACT 2019, 2019. doi: 10.1109/ICOIACT46704.2019.8938464.

[28] L. C. Paul and M. M. Islam, “A Super Wideband Directional Compact Vivaldi Antenna for Lower 5G and Satellite Applications,” Int J Antennas Propag, vol. 2021, 2021, doi: 10.1155/2021/8933103.

[29] P. J. Gibson, “VIVALDI AERIAL.,” in Conference Proceedings - European Microwave Conference, 1979. doi: 10.1109/euma.1979.332681.

[30] K. S. Yngvesson, D. H. Schaubert, T. L. Korzeniowski, E. L. Kollberg, T. Thungren, and J. F. Johansson, “Endfire Tapered Slot Antennas on Dielectric Substrates,” IEEE Trans Antennas Propag, vol. 33, no. 12, 1985, doi: 10.1109/TAP.1985.1143542.

[31] E. Gazit, “IMPROVED DESIGN OF THE VIVALDI ANTENNA.,” IEE Proceedings H: Microwaves, Antennas and Propagation, vol. 135, no. 2, 1988, doi: 10.1049/ip-h-2.1988.0020.

[32] J. D. S. Langley, P. S. Hall, and P. Newham, “Novel ultrawide-bandwidth Vivaldi antenna with low crosspolarisation,” Electron Lett, vol. 29, no. 23, 1993, doi: 10.1049/el:19931336.

[33] F. Etesami, S. Khorshidi, S. Shahcheraghi, and A. Yahaghi, “Improvement of radiation characteristics of balanced antipodal vivaldi antenna using transformation optics,” Progress In Electromagnetics Research M, vol. 56, pp. 189–196, 2017, doi: 10.2528/PIERM17013102.

[34] N. Hamzah and K. A. Othman, “Designing Vivaldi Antenna with various sizes using CST Software,” in Proceedings of the World Congress on Engineering 2011, WCE 2011, 2011.

[35] M. M. Rana, R. Khanom, and M. M. Rahman, “Design and Analysis of Vivaldi Antennas,” in 2018 International Conference on Innovation in Engineering and Technology, ICIET 2018, 2018. doi: 10.1109/CIET.2018.8660793.

[36] I. Guzelkara and V. T. Kilic, “Bandwidth Optimization of a Designed Ultra Wide Band Vivaldi Antenna with Its Feed Alignment,” unpublished.

[37] D. Pozar, Microwave Engineering Fourth Edition. 2005. doi: TK7876.P69 2011.

[38] C. Deng and Y. J. Xie, “Design of resistive loading Vivaldi antenna,” IEEE Antennas Wirel Propag Lett, vol. 8, 2009, doi: 10.1109/LAWP.2009.2013730.

[39] C. Zhao, X. Li, M. Yang, and C. Sun, “Resistance-loaded miniaturized dual-layer Vivaldi antenna for plasma reflection diagnosis,” Microw Opt Technol Lett, vol. 63, no. 1, 2021, doi: 10.1002/mop.32558.

[40] J. Ao, J. Huang, W. Wu, and N. Yuan, “A miniaturized Vivaldi antenna by loading with parasitic patch and lumped resistor,” AEU - International Journal of Electronics and Communications, vol. 81, 2017, doi: 10.1016/j.aeue.2017.07.022.

[41] M. Amiri, F. Tofigh, A. Ghafoorzadeh-Yazdi, and M. Abolhasan, “Exponential Antipodal Vivaldi Antenna with Exponential Dielectric Lens,” IEEE Antennas Wirel Propag Lett, vol. 16, 2017, doi: 10.1109/LAWP.2017.2679125.

[42] X. X. Li, D. W. Pang, H. L. Wang, Y. M. Zhang, and G. Q. Lv, “Dielectric slabs covered broadband Vivaldi antenna for gain enhancement,” Progress In Electromagnetics Research C, vol. 77, 2017, doi: 10.2528/PIERC17070308.

[43] A. Bhattacharjee, A. Bhawal, A. Karmakar, A. Saha, and D. Bhattacharya, “Vivaldi antennas: A historical review and current state of art,” 2021. doi: 10.1017/S1759078720001415.

[44] A. Chaabane and M. Guerroui, “A Planar Dual Notched Band Vivaldi Antenna for Wireless Communication Applications,” Def Sci J, vol. 74, no. 1, 2024, doi: 10.14429/dsj.74.19154.

[45] S. Saleh, W. Ismail, I. S. Z. Abidin, M. H. Jamaluddin, M. H. Bataineh, and A. S. Alzoubi, “Compact UWB Vivaldi Tapered Slot Antenna,” Alexandria Engineering Journal, vol. 61, no. 6, 2022, doi: 10.1016/j.aej.2021.09.055.

[46] J. Shin and D. H. Schaubert, “A parameter study of stripline-fed vivaldi notch-antenna arrays,” IEEE Trans Antennas Propag, vol. 47, no. 5, 1999, doi: 10.1109/8.774151.

[47] E. M. Khusna, E. Setijadi, and G. Hendrantoro, “Parameter study of coplanar vivaldi antenna feeding structure,” in Proceedings - 2019 International Seminar on Intelligent Technology and Its Application, ISITIA 2019, 2019. doi: 10.1109/ISITIA.2019.8937160.

[48] J. H. Shafieha, J. Nourinia, and C. Ghobadi, “PROBING THE FEED LINE PARAMETERS IN VIVALDI NOTCH ANTENNAS,” Progress In Electromagnetics Research B, vol. 1, 2008, doi: 10.2528/pierb07102702.

[49] K. Chung, S. Pyun, and J. Choi, “Design of an ultrawide-band TEM horn antenna with a microstrip-type balun,” IEEE Trans Antennas Propag, vol. 53, no. 10, 2005, doi: 10.1109/TAP.2005.856396.

[50] M. Moosazadeh, S. Kharkovsky, J. T. Case, and B. Samali, “Antipodal Vivaldi antenna with improved radiation characteristics for civil engineering applications,” IET Microwaves, Antennas and Propagation, vol. 11, no. 6, 2017, doi: 10.1049/iet-map.2016.0720.

[51] J. Eichenberger, E. Yetisir, and N. Ghalichechian, “High-Gain Antipodal Vivaldi Antenna with Pseudoelement and Notched Tapered Slot Operating at (2.5 to 57) GHz,” IEEE Trans Antennas Propag, vol. 67, no. 7, 2019, doi: 10.1109/TAP.2019.2906008.

[52] Z. Briqech, A. Sebak, and T. A. Denidni, “High gain 60 GHz antipodal fermi tapered slot antenna with sine corrugation,” Microw Opt Technol Lett, vol. 57, no. 1, 2015, doi: 10.1002/mop.28772.

[53] M. Abbak, M. N. Akinci, M. Çayören, and I. Akduman, “Experimental microwave imaging with a novel corrugated vivaldi antenna,” IEEE Trans Antennas Propag, vol. 65, no. 6, 2017, doi: 10.1109/TAP.2017.2670228.

[54] B. Sivashanmugavalli and B. Vijayalakshmi, “Performance measures of Vivaldi antenna with parasitic elements,” in Proceedings of the 2017 International Conference on Wireless Communications, Signal Processing and Networking, WiSPNET 2017, 2017. doi: 10.1109/WiSPNET.2017.8299712.

[55] I. T. Nassar and T. M. Weller, “A Novel Method for Improving Antipodal Vivaldi Antenna Performance,” IEEE Trans Antennas Propag, vol. 63, no. 7, 2015, doi: 10.1109/TAP.2015.2429749.

[56] Y. Tong, W. Cao, C. Wang, W. Ma, and S. Zhu, “A Miniaturized and Ultra-Wideband Antipodal Vivaldi Antenna With Triangular Slots,” in 2022 IEEE 10th Asia-Pacific Conference on Antennas and Propagation, APCAP 2022 - Proceedings, 2022. doi: 10.1109/APCAP56600.2022.10069509.

[57] Z. Li, X. Kang, J. Su, Q. Guo, Y. L. Yang, and J. Wang, “A Wideband End-Fire Conformal Vivaldi Antenna Array Mounted on a Dielectric Cone,” Int J Antennas Propag, vol. 2016, 2016, doi: 10.1155/2016/9812642.

[58] B. Tütüncu, H. Torpi, and B. Urul, “A comparative study on different types of metamaterials for enhancement of microstrip patch antenna directivity at the Ku-band (12 GHz),” Turkish Journal of Electrical Engineering and Computer Sciences, vol. 26, no. 3, 2018, doi: 10.3906/elk-1711-50.

[59] A. S. Dixit and S. Kumar, “A Survey of Performance Enhancement Techniques of Antipodal Vivaldi Antenna,” 2020. doi: 10.1109/ACCESS.2020.2977167.

[60] X. Zhang, Y. Chen, M. Tian, J. Liu, and H. Liu, “A compact wide-band antipodal Vivaldi antenna design,” International Journal of RF and Microwave Computer-Aided Engineering, vol. 29, no. 4, 2019, doi: 10.1002/mmce.21598.

[61] F. Shan, H. Huo, J. Zeng, Z. Li, W. Wu, and J. Luo, “Ultra-Wideband Swarm Ranging Protocol for Dynamic and Dense Networks,” IEEE/ACM Transactions on Networking, vol. 30, no. 6, 2022, doi: 10.1109/TNET.2022.3186071.

[62] J. H. Choi, J. E. Kim, and K. T. Kim, “People counting using ir-uwb radar sensor in a wide area,” IEEE Internet Things J, vol. 8, no. 7, 2021, doi: 10.1109/JIOT.2020.3032710.

[63] P. Sun, H. Zhang, and X. Liu, “Development and application of emergency rescue command system based on UWB technology,” in Proceedings - 2019

International Conference on Electronic Engineering and Informatics, EEI 2019, 2019. doi: 10.1109/EEI48997.2019.00067.

[64] D. Harmer et al., “A ultra-wide band indoor personnel tracking system for emergency situations (europcom),” in 2008 5th European Radar Conference Proceedings, EuRAD 2008, 2008.

CURRICULUM VITAE

2014 – 2021	B.Sc., Electrical and Electronics Engineering, Abdullah Gul University, Kayseri, TURKEY
2021 – Present	M.Sc., Electrical and Computer Engineering, Abdullah Gul University, Kayseri, TURKEY